

---

## CHAPTER 3

# Calculation of the Electronic Spectra of Large Molecules

**Stefan Grimme**

*Theoretische Organische Chemie, Organisch-Chemisches  
Institut der Universität Münster, Corrensstraße 40,  
D-48149 Münster, Germany*

---

---

### INTRODUCTION

With the development of more sophisticated quantum chemical methods in recent years, realistic calculations of molecular excited states became increasingly feasible. Electronically excited molecules play important roles in flames, plasmas, the atmosphere, and photochemical synthesis. Large organic molecules that absorb or emit in the visible region of the electromagnetic radiation spectrum are used as dyes or fluorescent markers in biological processes. The photochemistry of living systems, namely photosynthesis and the vision process, are currently under intense investigation. All these phenomena require (at least initially) a detailed consideration of the spectral properties of the excited states involved.

Electronic spectra arise from transitions between electronic states of different quantum numbers induced by electromagnetic radiation with ultraviolet or visible (UV/vis) light. The term “electronic spectra” implies the Born–Oppenheimer (BO) picture of molecules where the electronic and nuclear degrees of freedom are separated. Similarly, the description of the spectra in terms of particular electronic states is valid solely in a small region of the

nuclear configuration space, that is, for chemically similar structures. Each excited state has, in all respects, different properties than the ground state, namely, energy, geometry, electron density, dipole moment, and so on. In this sense, we can consider the excited states of one molecule as different types of entities or occurrences of the same Hamiltonian.

Excited states are very important in quantum chemistry. Obviously, they are the basic quantities of interest when electronic spectra are considered. Furthermore, because the excited states form a complete basis of the Hamiltonian, all second-order properties such as polarizabilities (van der Waals forces), NMR chemical shifts, ESR  $g$ -tensors, or optical rotations of chiral molecules can be calculated quite accurately by sum-over-(excited) state expressions. It should also be clear that any attempt to model photochemical reactions must be preceded by a careful examination of the electronic spectra of the reactants and products in order to deduce the electronic character of the states involved.

The interpretation of electronic spectra is more difficult than those obtained by IR or NMR techniques and also the theoretical–computational requirements are higher. The reason for this is that usually a significant reorganization of the electronic and nuclear coordinates occurs upon excitation and, in addition, the induced changes are often delocalized in nature. Furthermore, even for medium-sized systems, the density of states in small energy regions can be very large, which leads to overlapping spectral features (due to large band widths). These features are theoretically (and also experimentally) difficult to resolve.

The ability of electronic structure theory to make reliable predictions for excitation energies and transition moments has advanced extraordinarily in recent years. By using time-dependent density functional theory (TDDFT), linear-response (LR) or equation-of-motion (EOM) coupled-cluster (CC), or multireference perturbation theory (MRPT), even relatively large molecules now can be investigated routinely. On the other hand, investigations of excited-state problems are still not as routine as most ground states. Also, reliable “black-box” type methods to simulate a wide variety of electronic spectra are still missing. Although some of the problems may be solved in the near future by more efficient computer algorithms and advanced hardware capabilities, inherent difficulties in the description of excitation processes will remain. It seems obvious that the complexity of the problem requires more human efforts, that is, a careful examination and understanding of the system under consideration, and furthermore a bit more than basic knowledge about the theoretical methods that are used.

This chapter provides a comprehensive overview of the current status of computational chemistry to describe electronic spectra. The focus is predominantly on larger molecular systems under medium-to-low resolution conditions. A quantitative description of the high-resolution spectra of diatomic to four-atom molecules requires special treatments for vibrational and relativistic

fine-structure effects and must also employ highly accurate quantum chemical methods (e.g., multireference configuration interaction, MRCI), which are currently not feasible for larger molecules. The main intention of this presentation is to provide the nonspecialist with an introduction to the field and a review of the key references that may be helpful as a starting point for his or her own investigations.

After a very basic introduction to the problem in which the general types of spectra and excited states are discussed, various theoretical aspects of the simulation of electronic spectra are outlined in the following section. This section includes the important topics of excitation energies and transition moments as well as some consideration of vibrational effects that can now be included routinely even for larger systems. It also includes a comprehensive but condensed presentation of quantum chemical methods that can, and should, be applied to these problems. The last section contains case studies of a variety of problems including UV spectra of organic and transition metal systems, Rydberg spectra, spectra of open-shell systems, and circular dichroism (CD) spectroscopy, which also involves magnetic transition moments. In addition, recent advances in the description of vibrational structure in the electronic spectra of larger molecules are described.

Before continuing, we want to refer the reader to some of the existing reviews and key references about this topic. Many of the general theoretical and technical aspects of quantum chemical methods cannot be considered here. In this respect, the reader is referred to the excellent book of Helgaker et al.<sup>1</sup> The most recent introduction to the problem of electronic spectroscopy is that of Peyerimhoff,<sup>2</sup> where many important older references can also be found. Much older, but still valuable books, are those of Murrell,<sup>3</sup> Jaffe and Orchin,<sup>4</sup> Mataga and Kubota,<sup>5</sup> and Robin.<sup>6</sup> The standard textbooks on photochemistry from Turro,<sup>7</sup> Michl and Bonacic-Koutecky,<sup>8</sup> and Klessinger and Michl<sup>9</sup> also include good introductions to the theoretical description of electronic spectra. More specific reviews, that is, those dealing with a particular theoretical method (such as CASPT2) can be found in the excellent contributions from the Roos group.<sup>10–12</sup> A recent review of electronic excitations in aggregates—oligomers including density matrix based techniques to analyze the states has recently been given by Tretiak and Mukamel.<sup>13</sup> A very good survey of spin–orbit effects on electronic spectra (not considered here), which emphasizes theoretical aspects, has recently been given by Marian<sup>14</sup> (see also Ref. 15).

## Types of Electronic Spectra

To perform reliable quantum chemical simulations of electronic spectra, a detailed understanding of the different state and possible transition types is necessary. Figure 1 provides a schematic overview of the processes usually observed for molecules where, for simplicity, the rovibrational fine structure of the electronic levels has been neglected.

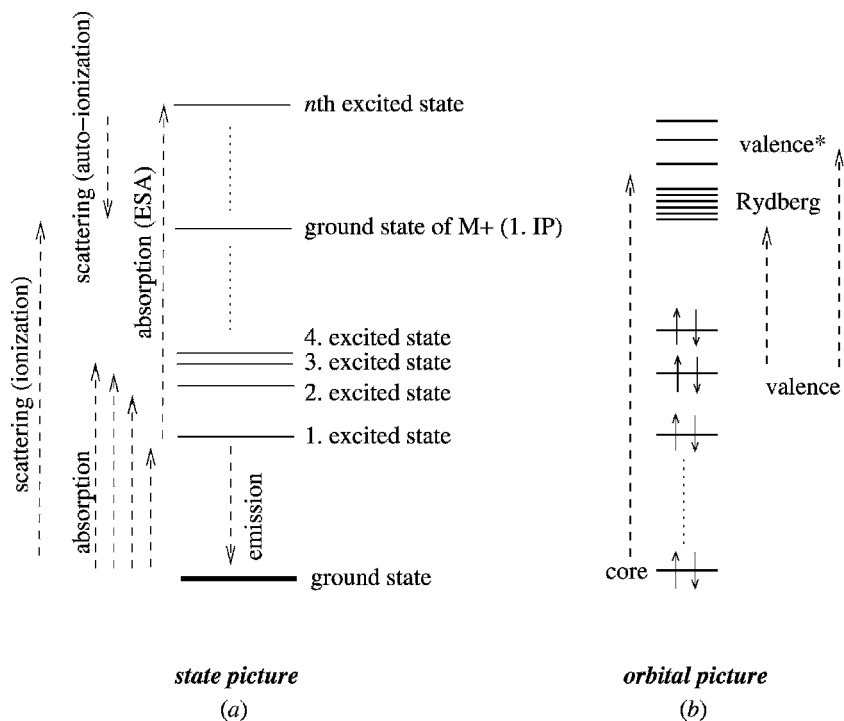


**Figure 1** Overview of different state and transition types in a state (a) and orbital picture (b). Abbreviations: IP (ionization potential), ESA (excited-state absorption).

One of the key points here is that state and orbital pictures should not be interchanged or mixed. Electronic absorption spectra originate from transitions between eigenstates and *not* from those between one-electron wave functions (orbitals). While the state picture is exact, but provides no detailed information about the electronic structures, the orbital picture is approximate. However, it is intuitively understandable and allows for easy classification of electronic spectra. In the orbital picture, a transition between the ground and an excited state is simplified to an excitation between origin (occupied in the ground state) and target (virtual, i.e., usually empty in the ground state) orbitals. More mathematically speaking, one implicitly uses single excitations between the orbitals (even more precisely: singly substituted Slater determinants; the terms “excited” and “substituted” are used synonymously) to express the wave functions of the excited states. Beside the most common valence–valence excitations, valence–Rydberg excitations are important in which the final orbital has relatively large spatial extent resembling atomic functions of higher principal quantum number. Core excitation spectra are an important tool in material science for the assignment of molecular oxidation states [for a very early and the most recent density functional theory (DFT) study on this topic see Refs. 16 and 17].

The dominating importance of single excitations is based on physical reasons. They dominate the most common one-photon processes, since they usually have low excitation energies and involve large transition moments (intensities). This is different for two-photon spectra; for a recent DFT study on this topic, see Ref. 18.

The large number of excitation possibilities, especially in higher lying energy regions, is one of the reasons why absorption spectra simulations are so difficult. Because emission processes are usually observed only from the lowest excited state to the ground state (in rare cases a second excited state must be considered), their theoretical description is much easier. Energetically embedded into the electronic spectrum are ionic states, where at least one electron has been removed from the system. These continuum states and their formation are the topic of scattering theory, which will not be considered here. However, especially for Rydberg spectra, ionized states are important because they represent the asymptotic limit of a Rydberg series with infinite principal quantum number.

The second important issue to consider is the measurement conditions under which the experimental spectra are recorded. This not only has dramatic consequences for the shape of the spectra but also determines which theoretical approaches should be taken. Figure 2 shows different visible absorption

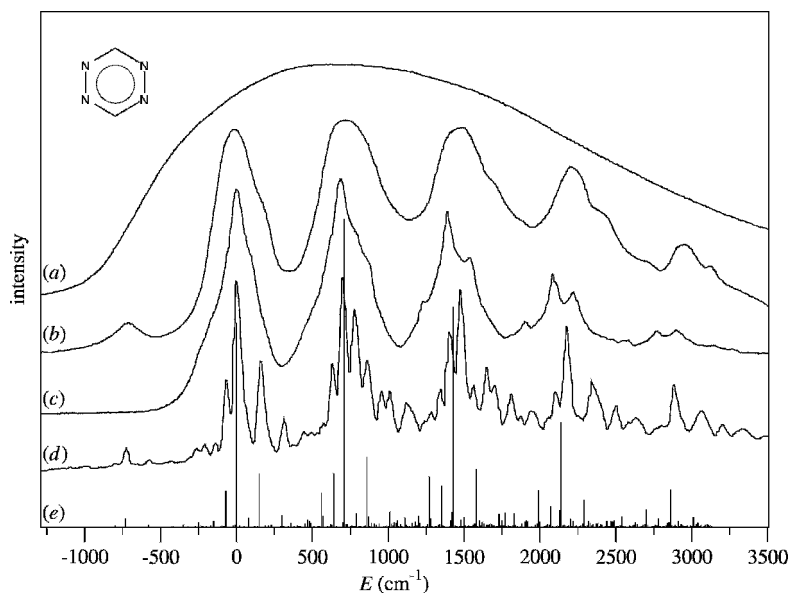


**Figure 2** Visible absorption spectra ( $n \rightarrow \pi^*$  state, onset at  $\sim 550$  nm) of tetrazine under different conditions (from top to bottom): (a) aqueous solution at room temperature (RT), (b) cyclohexane at RT, (c), hydrocarbon matrix at 77 K, (d) gas phase at RT, and (e) TDDFT-B3LYP<sup>20,21</sup> simulation of the vibronic transitions at RT. The 0-0 vibronic transition has been set to zero.

spectra for the  $n \rightarrow \pi^*$  band of tetrazine, where the influence of environment and temperature can be seen very clearly (this nice example was first presented by Mason<sup>19</sup>).

Spectrum (*d*) shows a medium-resolved UV spectrum in the gas phase at room temperature for which a huge number of vibronic transitions occurring simultaneously with the change of electronic quantum number are resolved. A detailed understanding of this spectrum including hot-bands (excitations out of vibrationally excited levels of the ground state, excitation energies  $< 0$  in Figure 2) requires a vibrational treatment of both electronic states. Trace (*e*) shows the result of such a simulation (outlined in more detail in later sections) presented as a “stick-spectrum,” which is in almost perfect agreement with experiment. Due to solvent–matrix-induced line-broadening, the fine structure is clearly reduced in the spectrum that is recorded in a hydrocarbon matrix at low temperatures. Note the missing hot band, for example, at  $-700\text{ cm}^{-1}$  due to decreasing population of thermally excited vibrational levels in the ground state. With increasing temperature (spectrum *b*), the density of vibrational states increases thereby further broadening the bands. It seems clear that changes of this kind require the inclusion of temperature in the simulations, for example, via population of levels according to a Boltzmann distribution. The spectra (*b*) and (*c*) have been recorded in weakly interacting hydrocarbon solvents that more or less resemble the gas-phase spectrum. Experience shows that such spectra can be safely used in theoretical treatments (which mostly neglect solvent effects) as substitutes for the often missing gas-phase spectra. In most cases, weakly interacting solvents just induce a small red-shift of the entire spectrum due to a higher polarizability (larger stabilization by van der Waals interactions) of the excited states. On the contrary, spectrum (*a*) recorded in water shows complete loss of any vibrational structure due to strong interactions with the solvent (mostly weak  $\text{N} \cdots \text{H}$  bonds). This situation would require the calculation of a number of different water–tetrazine aggregates, including their dynamic behavior, which is currently out of reach for any reliable quantum mechanical treatment.

## Types of Excited States

Selection of the theoretical method to be employed in practical simulations is the decisive factor for the overall accuracy of a calculated spectrum. The main problem in computing the various electronic states is to properly account for the electron correlation (EC) effects, which is the difference between a Hartree–Fock (HF) independent particle model and reality. Usually, one distinguishes between dynamic (short-ranged) EC, which is ubiquitous and can be understood as a pure many-particle effect, and static (long-ranged) EC resulting from the energetic near-degeneracy of different electronic configurations. This very important issue is outlined schematically in Figure 3. Note that in the following we deal exclusively with spin-allowed transitions (i.e., no

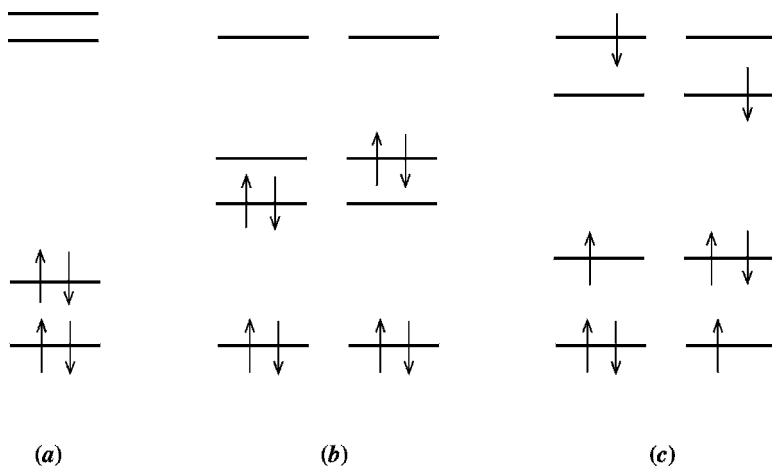


**Figure 3** Orbital pictures of electron correlation effects: (a) ground state of a closed-shell system with a large highest occupied molecular orbital–lowest unoccupied molecular orbital (HOMO–LUMO) gap showing predominantly dynamic EC. (b) Near-degeneracy of two electronic configurations occurring, for example, in biradicals or during homolytic bond cleavage. (c) Near-degeneracy of two singly substituted electronic configurations in an excited state.

change of spin-multiplicity between the states) and that mostly even-numbered electron systems with singlet multiplicity will be discussed (exceptions are the phenoxy radical and the lowest triplet state of naphthalene, both discussed in a later section).

Electronic excitation is usually connected with an unpairing of electrons, which, as a rule of thumb, contributes  $\sim 1$  eV correlation energy change per pair. Furthermore, even the usual definition of the correlation energy ( $E_{\text{corr}} = E_{\text{exact}} - E_{\text{HF}}$ ) is not unambiguous for excited states because a HF self-consistent field (SCF) description (which is used as “uncorrelated” reference) is rarely possible. Because the degree of sophistication of the theoretical treatment that can be performed is usually limited, it is important to know which main factors influence the magnitude of the electron-correlation contributions.

For that purpose, electronic spectra are first classified according to the character of the states involved. A very basic distinction relies on the electronic structure of the corresponding initial state from which the transition occurs. This initial state is not necessarily the ground state of the system, shown schematically in Figure 4, which includes the three most common possibilities. For a more detailed discussion of this point in the context of restricted and unrestricted TDDFT approaches, see Ref. 22.

Most electronic spectra are measured for closed-shell systems that usually have a large gap between occupied and virtual orbitals. This case is the

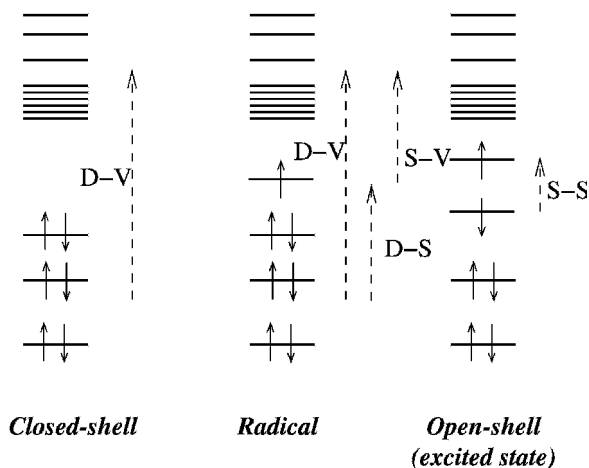


**Figure 4** Orbital pictures of the most common initial-state configurations and the different types of single excitations. The open-shell state shown on the right side additionally has the possibility of *S-S* excitations. Abbreviations: doubly occupied MO (D), virtual MO (V), singly occupied MO (S).

simplest because the initial state is then often the ground state of the system (we consider absorption here) and it is, furthermore, usually well described by a single Slater determinant. In these systems, doubly occupied MO to virtual MO (*D-V*) single excitations (see Figure 4) play the most important role, although important exceptions with low-energy double excitations (e.g., polyenes) are known. It is clear that the number of different excitation types increases for systems that are already open shell in the ground state. For radicals, doubly occupied to singly occupied (*D-S*) and singly occupied to virtual (*S-V*) excitations must also be considered and in the case of excited-state absorption, *S-S* excitations are also possible. While many different theoretical approaches have been developed and extensively tested for the closed-shell situation, the open-shell systems are more complex. For low-spin states especially, only a few methods are, in principle, applicable.

Table 1 contains a state classification in terms of the more chemically-physically motivated language often used in the literature. Note that the entries in the different sections can in fact occur in almost arbitrary combinations, for example a charge-transfer excited state can be single reference dominated by single excitations (a state often occurring lowest in dyes) or one can have a high-spin Rydberg state, and so on. The last column contains theoretical issues that may be applicable in particular cases.

As already mentioned, the accurate account of the electron correlation effects in the different states is the most important precondition to obtain reliable predictions for electronic spectra. Before considering some details of this simulation process, a few words on general aspects of EC in larger systems

**Table 1** Overview of Excited-State Types<sup>a</sup>

State Classification	Description	Theoretical Aspects to Consider
<i>Valence</i>	Excitations between (non)bonding–anti-bonding orbitals	Strongly varying amounts of EC
<i>Rydberg</i>	Excitations to virtual orbitals of large spatial extent	Special AO basis sets required asymptotics of potential <sup>b</sup>
<i>Core excited</i>	Excitations out of core orbitals	Special treatments–algorithms to extract high-lying roots
<i>Locally excited</i>	Excitations between spatially close orbitals	
<i>Charge transfer</i>	Excitations between very distant orbitals	Asymptotics of potential <sup>b</sup>
<i>Singly excited</i>	WF are dominated by singly excited determinants	Simple TD approaches sufficient <sup>c</sup>
<i>Multiply excited</i>	WF includes important contributions from doubles, triples, and so on	Multireference approaches necessary
<i>Single reference</i>	WF can be described mainly by one determinant	Mostly dynamic EC
<i>Multi-configurational (multireference)</i>	WF includes many important contributions	Breakdown of MO picture Static EC
<i>Low spin</i>	Spins are mostly paired (e.g., singlet, doublet)	EC larger for low-spin than for high-spin states
<i>High spin</i>	$M_s > M_s(\text{min})$ (e.g., triplet, quartet)	

<sup>a</sup>Abbreviations: WF (wave function), EC (electron correlation), TD (time-dependent), AO (atomic orbital).

<sup>b</sup>Mainly apply to TDDFT, where approximate exchange-correlation potentials are used in the effective Kohn–Sham Hamiltonian.

<sup>c</sup>For example, adiabatic TDDFT or LR(EOM) coupled-cluster singles and doubles.

seem appropriate. Large molecules are close to a crossover region when going from molecular systems to solids, and, from a physicist's point of view would be classified as insulators, semiconductors, or metals. The EC effects in insulators (saturated with  $\sigma$ -bonds only) are mostly local (short-ranged, dynamic) in nature and can thus be described by local wave function or density functional methods. The variations of the EC effects between the different states of insulators are expected to be small or roughly constant so that even simple methods completely lacking EC may be sufficient. However, these simple systems are not very interesting chemically and, thus, most theoretical treatments performed in practice must consider semiconductor- or even metal-like molecules. One characteristic of the states in these systems is the nonlocality of

the EC (or even exchange) effects, where also a separation into static and dynamical EC is no longer appropriate. This nonlocality is difficult to describe theoretically mainly because (a) three or more particle correlations become important and (b) theoretical approximations that rely on “spatial separation” cannot be used. Thus, only correlated wave function approaches that include these effects explicitly will ultimately yield the desired accuracy in these cases. In this context, a strong warning should be noted: For obvious reasons, most developments of new quantum chemical methods for excited states will be tested and “benchmarked” on atoms or small molecules with only a few electrons. The results and conclusions thus obtained are not always transferable to “real” problems (i.e., a method that gives good results for ethene is not necessarily appropriate for porphyrin) mostly because the importance of higher order EC effects increases with the size of the system.

---

## THEORY

### Excitation Energies

In the Born-Oppenheimer picture, electronic transitions occur between rovibrational levels of two electronic states  $n$  and  $m$ . The excitation energy is the energy difference between the two levels yielding the spectral position of the transition

$$\Delta E_{nm, \nu \nu', j j'} = E_{m, \nu', j'} - E_{n, \nu, j} \quad [1]$$

where  $\nu$  and  $j$  indicate vibrational and rotational quantum numbers, respectively. Because the rotational structure is rarely resolved experimentally for larger molecules, we always assume in the following that  $j = j' = 0$  and drop the corresponding index. For the special case that the transition occurs between the two vibrational ground states ( $\nu = \nu' = 0$ ), Eq. [1] reduces to

$$\Delta E_{nm}^{0-0} = E_m^{\text{el}} - E_n^{\text{el}} + E_m^{\text{ZPE}} - E_n^{\text{ZPE}} \quad [2]$$

yielding the 0–0 transition energy  $E^{0-0}$ , where  $E^{\text{ZPE}}$  are the vibrational zero-point energies. At low temperatures, the 0–0 transition can usually be identified as the onset of the experimental spectrum. The calculation of this important quantity thus requires the computation of the two electronic-state energies and their vibrational normal modes. Because the calculation of  $E^{\text{ZPE}}$  is relatively demanding (even in the usually employed harmonic approximation), one often replaces the 0–0 transition energy by the pure electronic part,

$$\Delta E_{nm}^{\text{el}} = E_m^{\text{el}} - E_n^{\text{el}} \quad [3]$$

This approximation is relatively accurate yielding errors typically  $< 0.1$ – $0.2$  eV. If transitions from the ground state are considered, these errors are systematic because the vibrational frequencies in the excited state are usually smaller than in the ground state and thus,  $\Delta E^{\text{el}} > \Delta E^{0-0}$ .

So far, all energies discussed for the two states necessarily refer to energy minima, and thus, two separate geometry optimizations of the molecular structures are required. While this is a routine task for most ground states, excited-state geometry optimization is a very difficult problem. First, for most of the more accurate excited-state quantum chemical models, implementations of analytical gradients are still missing. Although numerical derivatives can in principle always be obtained, their calculation is usually too costly and thus they are used only for benchmark purposes on small systems.<sup>2,3</sup> Second, in higher energy regions, the density of states is usually very large, which leads to many avoided surface crossings. In such situations, geometry optimizations are almost impossible because state flippings often occur and induce a complete breakdown of the most common quasi-Newton optimization algorithms. These are the reasons that even today most investigations rely on the so-called vertical approximation. In this approach, the optimized ground-state geometry is used to calculate all excited-state energies and transition moments. Note that the vertical excitation energy

$$\Delta E'_{nm}{}^{\text{el}} = E'_m{}^{\text{el}} - E_n{}^{\text{el}} \quad [4]$$

(where the prime indicates the use of the nonrelaxed ground-state geometry) does not correspond to any observable. Instead, it represents a relatively good approximation (often to within  $0.1$ – $0.2$  eV) to the intensity maximum of a spectral band. It should be clear that this approach works best for large molecules with small geometry changes between the states and for spectra obtained in solution under low-resolution conditions. Typical values for the difference between vertical and  $0-0$  excitation energies are given in Table 3.

The ultimate goal of theoretical electronic spectroscopy is to provide reliable and realistic simulations of electronic spectra. For that purpose, one usually needs a relatively high accuracy for the excitation energies. If we consider valence and Rydberg states with  $\Delta E$  values of  $< 10$  eV, and if we assume typical bandwidths of  $\sim 0.3$ – $0.5$  eV, the errors for  $\Delta E$  should not exceed  $0.2$ – $0.3$  eV. Even more important than the accuracy of the absolute values (systematic errors can be corrected by global shifting or scaling as is usually done in IR spectroscopy) is the relative accuracy obtained for the different states of one molecule. A wrong ordering of states can lead especially to misinterpretation of experimental data, an issue that is a particular problem in photochemical studies.

To illustrate the accuracy that can be obtained by modern quantum chemical methods, the results for a benchmark set of molecules is now briefly discussed. An outline of the theoretical background of the applied methods is

**Table 2** Comparison of Calculated Vertical Singlet–Singlet Excitation Energies with Experimental Absorption Band Maxima<sup>a</sup>

Molecule	State	Experimental (eV)	TDDFT-B3LYP	CC2	MR-MP2
			Error <sup>b</sup> (eV)		
Anthracene	$1^1B_{3u}(\pi\pi^*, L_a)$	3.3	0.03	0.69	0.39
	$1^1B_{2u}(\pi\pi^*, L_b)$	3.5	0.42	0.43	-0.15
Indole	$2^1A'(\pi\pi^*, L_b)$	4.4	0.52	0.53	-0.15
	$3^1A'(\pi\pi^*, L_a)$	4.8	-0.02	0.47	0.15
Porphyrin	$1^1B_{1u}(\pi\pi^*)$	2.0	0.08	0.32	-0.33
	$1^1B_{2u}(\pi\pi^*)$	2.4	0.05	0.31	-0.07
	$2^1B_{1u}(\pi\pi^*)$	3.1	0.24		-0.03
	$2^1B_{2u}(\pi\pi^*)$	3.3	0.22		-0.02
Indigo	$1^1B_u(\pi\pi^*)$	2.0	0.08	0.36	0.10
Pyridazine	$1^1B_2(n \rightarrow \pi^*)$	3.4	0.14	0.47	0.22
Benzocyclo- butendione	$1^1B_2(n \rightarrow \pi^*)$	2.8	0.10	0.19	-0.12
Benzaldehyde	$1^1A_2(n \rightarrow \pi^*)$	3.5	0.05	0.33	0.12
	$1^1A''(n \rightarrow \pi^*)$	3.8	-0.17	0.12	0.18
C <sub>5</sub>	$\Pi_u(n \rightarrow \pi^*)$	2.8	0.56		-0.19
Pyrrole	$1^1A_2(\pi \rightarrow 3s)$	5.2	-0.45	-0.06	0.06
	$1^1B_2(\pi \rightarrow 3p)$	5.9	-0.36	-0.10	0.10
Si <sub>2</sub> (CH <sub>3</sub> ) <sub>6</sub>	$1E_u(\sigma \rightarrow 4p)$	6.4	-0.38	-0.68	0.12
Ferrocene	$1^1E_{1g}(d \rightarrow d)$	2.8	-0.79		-0.09
Cr(CO) <sub>6</sub>	$1^1T_{1u}(d \rightarrow \pi^*)$	4.4	0.08		0.34
	$2^1T_{1u}(d \rightarrow \pi^*)$	5.5	0.50		0.10
P <sub>4</sub>	$1^1T_2$	5.6	-0.08	-0.08	-0.22
Na <sub>4</sub>	$1^1B_{3u}$	1.8	0.06	0.03	0.05
mean absolute deviation (MAD)			0.24	0.32	0.15

<sup>a</sup>For technical details and references to the experimental data see Ref. 25.<sup>b</sup>Error =  $\Delta E(\text{calc.}) - \Delta E(\text{exp.})$ .

given in a later section. Table 2 shows results for vertical singlet–singlet excitation energies obtained with TDDFT (time-dependent density functional theory), CC2 (a simplified coupled-cluster model), and MR-MP2 methods (multireference perturbation theory). The systems tabulated have been chosen to cover a broad range of molecules and states of different character. Further discussions on the accuracy of calculated  $\Delta E$  values are given below in the sections containing the case studies; another TDDFT benchmark study can be found in Ref. 24.

Inspection of the data clearly shows how difficult it is to meet the accuracy requirements of  $\sim 0.2$ – $0.3$  eV even for these lowest-lying states. Although the mean absolute deviation (MAD) for all three methods falls in this range, only the MR-MP2 method achieves a good overall accuracy for the entire range of systems. Both TDDFT and CC2 have some outliers with errors

>0.5 eV and CC2, especially, completely breaks down for  $C_5$  and the difficult transition metal systems. Note that the three methods tested represent the most accurate approaches that can also be applied to larger systems and that other “cheap” methods (like CIS or semiempirical treatments) often yield quite unreliable results with errors >0.5–1 eV.

As already mentioned, a direct comparison of vertical excitation energies with experimental data is not possible and such results contain uncertainties due to geometry relaxation effects. A more reliable assessment of theoretical methods can be achieved by a comparison of the  $\Delta E^{0-0}$  values that are presented for the lowest states of some unsaturated molecules in Table 3. The last column of this table indicates the difference between 0–0 and vertical excitation energies.

These data indicate more clearly the problems theoretical methods (TDDFT in this case) have in accounting for the change of electronic structure upon excitation. For the ionic  $L_a$  states of the aromatic compounds (using Platts nomenclature derived from the perimeter model, see, Ref. 9 e.g.) and the  $1B_u$  state of the polyene, a systematic underestimation of the excitation energies is observed while the opposite is true for the other more covalent states that exhibit stronger multiconfigurational character (for a more detailed discussion of these problems see Refs. 35 and 36).

The effects of geometry relaxation (sixth column) are significant for the smaller and medium-sized systems (0.4–0.6 eV) but diminish with the size of the molecule. For the larger aromatic molecules, differences between  $\Delta E^{el}$  and  $\Delta E^{0-0}$  of  $\sim 0.2$ – $0.3$  eV are found. Note, however, that the geometry relaxation effects can be more important (up to 1 eV) in the case of larger systems as well when single-bond torsions between conjugated fragments are possible.<sup>37</sup> The differences between the  $\Delta E^{el}$  and  $\Delta E^{0-0}$  values (the ZPE contribution) are much smaller (0.12–0.17 eV, 0.03 eV for azulene) and roughly constant for the systems considered.

## Transition Moments

Band intensities (transition probabilities) are the second important factor determining the shape of an electronic spectrum. Including the oscillating radiation field as a perturbation to the molecular Hamiltonian and applying time-dependent perturbation theory yields, under some approximations (the most important being that the radiation wavelength is much larger than the size of the molecule and small field strengths), the electronic transition moment (TM) as an expectation value over the initial and final wave functions with the relevant one-electron operator  $\hat{O}$ ,

$$\text{TM} = \langle \Psi_m | \hat{O} | \Psi_n \rangle \quad [5]$$

**Table 3** Comparison of Calculated [TDDFT-B3LYP/TZV(d,p)] and Experimental 0–0 Excitation Energies (in eV) for the Lowest Singlet States ( $\pi\pi^*$ ) of Unsaturated Systems

Molecule	Transition	$\Delta E^{0-0}$			Error	$\Delta E^{\text{el}} - \Delta E^{0-0}$		Reference
		Calc.	Exp.	Error		Calc.	Conditions	
Naphthalene	$1B_{2u}, L_a$	3.98	4.44	-0.46	0.42	Gas phase	26	
Anthracene	$1B_{2u}, L_a$	2.90	3.43	-0.53	0.33	Gas phase	26	
Tetracene	$1B_{2u}, L_a$	2.18	2.77	-0.59	0.29	Argon jet	27	
Pentacene	$1B_{2u}, L_a$	1.66	2.12	-0.46	0.33	Hexadecane matrix	28	
Pyrene	$1B_{2u}, L_a$	3.43	3.84	-0.41	0.26	Gas phase	26	
Azulene	$1B_1$	1.99	1.78	0.21	0.41	Cyclohexane	29	
Octatetraene	$1B_u$	3.71	4.41	-0.70	0.34	Argon jet	30	
Octatetraene	$2A_g$	4.46	3.59	0.87	0.45	Helium jet	31	
Styrene	$2A'$	4.41	4.88	-0.46	0.56	Argon jet	32	
Phenol	$2A', L_b$	4.79	4.51	0.28	0.31	Argon jet	33	
o-Cyanophenol	$2A', L_b$	4.32	4.21	0.11	0.31	Helium jet	34	

A comprehensive discussion of this important derivation can be found in Refs. 38 and 39. The nuclear contributions to the TM leading to vibrational fine structure in the spectra are discussed in the following section. Alternatively, the electronic part of the TM is obtained from the first-order reduced transition density matrix  $\gamma$  as

$$\text{TM} = \text{tr}(\mathbf{O}\boldsymbol{\gamma}) \quad [6]$$

where the matrix  $\mathbf{O}$  is the representation of the operator in the basis of orbitals  $\psi$  ( $O_{ij} = \int \psi_i(r)\hat{O}\psi_j(r)dr$ ) and  $\boldsymbol{\gamma}$  is the analogous matrix representation of the transition density given by

$$\gamma_{ij} = \int \psi_i(r_1)\gamma(r_1, r'_1)\psi_j(r'_1)dr_1dr'_1 \quad [7]$$

with

$$\gamma(r_1, r'_1) = N_{\text{el}} \int \Psi_m \Psi_n dr_2 \cdots dr_N \quad [8]$$

The importance of the concept of transition density matrices is that they allow a straightforward interpretation of excited states<sup>13</sup> either by plotting or by population analyses as usually performed for “normal” ( $n = m$ ) densities.

The leading term in the interaction of radiation with matter is the electric dipole contribution ( $\boldsymbol{\mu}$ ) for which the one-electron operator  $\hat{O}$  is given by the position coordinates  $r_k$  of the electrons as

$$\hat{O} \equiv \hat{\boldsymbol{\mu}}_L = e \sum_k^{N_{\text{el}}} \hat{\mathbf{r}}_k \quad [9]$$

which is called the “dipole-length” form. Note that  $\boldsymbol{\mu}$  are vector quantities (given in bold) including  $x$ ,  $y$ , and  $z$  components. The alternative “velocity” formulation uses

$$\hat{O} \equiv \hat{\boldsymbol{\mu}}_V = \frac{-ie}{\Delta E^{\text{el}}} \sum_k^{N_{\text{el}}} \hat{\mathbf{v}}_k \quad [10]$$

For exact wave functions and those that fulfill the hyper-virial theorem by construction [e.g., time-dependent Hartree–Fock (TDHF) or random phase approximation (RPA), TDDFT, see below] both forms are equivalent. Note that all virial theorems are exactly fulfilled only in a complete (i.e., usually infinitely large) AO basis. By a simultaneous computation of the transition dipole moments in the length and velocity forms and subsequent numerical

**Table 4** The TDHF Transition Dipole Moments (in Debye) for the  $1^1A' \rightarrow 1^1A''$  Transition ( $n \rightarrow \pi^*$  excited state) in Acetaldehyde Calculated with Dunning's Correlation Consistent cc-VXZ Basis Sets<sup>a</sup>

Basis Set		$\mu_V$	$\mu_L$
cc-VDZ	[3s2p/2s]	0.0701	0.0363
cc-pVDZ	[3s2p1d/2s1p]	0.0072	0.0330
cc-pVTZ	[4s3p2d1f/3s2p1d]	0.0317	0.0534
aug-cc-pVTZ	[4s3p2d1f/3s2p1d] + [1s1p1d1f/1s1p1d]	0.0695	0.0674
cc-pVQZ	[5s4p3d2f1g/4s3p2d1f]	0.0513	0.0591
aug-cc-pVQZ	[5s4p3d2f1g/4s3p2d1f] + [1s1p1d1f1g/1s1p1d1f]	0.0675	0.0670

<sup>a</sup>See Refs. 40 and 41.

comparison, the above mentioned time dependent (TD) methods allow some estimate of basis set completeness for the corresponding transition. Table 4 provides a numerical comparison of the two transition dipole moments for the weakly allowed  $n \rightarrow \pi^*$  transition in acetaldehyde calculated with different AO basis sets.

It can be seen that if a certain degree of basis set saturation is reached (cc-pVTZ, third row), the two values start to converge to the same value ( $\sim 0.067$ ), which is almost reached at the aug-cc-pVTZ level. Note the strong effect of "diffuse" functions (denoted as aug) for this property (compare rows three/four and five/six) and also the relatively large fluctuations for the velocity form that are caused by the more complicated structure of the differential operator in Eq. [10]. In addition, there is a lot of numerical evidence that for other systems the length form is more stable yielding, with small AO basis sets, results closer to the basis set limit (see, e.g., Ref. 42). Note too that the presented example is quite challenging due to the "almost" symmetry forbidden character of the transition and that both the fluctuations for the V-form are smaller and the agreement between L- and V-forms is better for dipole allowed transitions.

The (dimensionless) oscillator strength for an electronic transition is given by

$$f_{nm} = \frac{2}{3} \Delta E_{nm} |\mathbf{\mu}_{nm}|^2 \quad [11]$$

where  $\Delta E$  and the length of the transition dipole vector are expressed in atomic units. Theoretically,  $f = 1$  corresponds to the transition probability of a harmonically moving electron bound to a proton (an early model of the hydrogen atom). Experimentally, one obtains  $f$  by integrating the area under the absorption band between energies  $\bar{\nu}_1$  and  $\bar{\nu}_2$  (in wavenumbers)

$$f = 4.3 \times 10^{-9} \int_{\bar{\nu}_1}^{\bar{\nu}_2} \epsilon(\bar{\nu}) d\bar{\nu} \quad [12]$$

where  $\varepsilon$  is the decadic molar extinction coefficient given in L/(mol cm). Although in experimental investigations a nonlinear energy scale  $\lambda = hc/E$  (wavelengths) is usually used, it is strongly recommended that one transform all data (experimental and theoretical) first to linear eV or  $\text{cm}^{-1}$  units. Inversion of Eq. [12] allows one to deduce  $\varepsilon(\bar{\nu})$  from calculated oscillator strengths. For the band form of the individual transitions (also called “shape-function”), Gaussian functions have been successfully employed, which accounts for vibrational (and solvent, if present) induced broadening. To simulate entire spectra, the contributions from all transitions are added according to

$$\varepsilon(E) = \frac{2.87 \times 10^4}{\sqrt{\sigma}} \sum_i f_i e^{[-(E-\Delta E_i)/2\sigma]^2} \quad [13]$$

where  $\sigma$  is the full width of the band at  $1/e$  height (for most UV bands  $\sigma = 0.4$  eV is appropriate) and  $\Delta E_i$  (in eV) and  $f_i$  are the excitation energies and oscillator strengths for transition  $i$ , respectively. Figure 5 schematically shows a typical outcome for the simulation of a conventional UV spectrum. The vertical lines indicate the position and oscillator strength of the individual transitions (right  $f$  axis), while the dashed curve is the overall result from Eq. [13]. Very weak or forbidden transition should be indicated by special symbols.

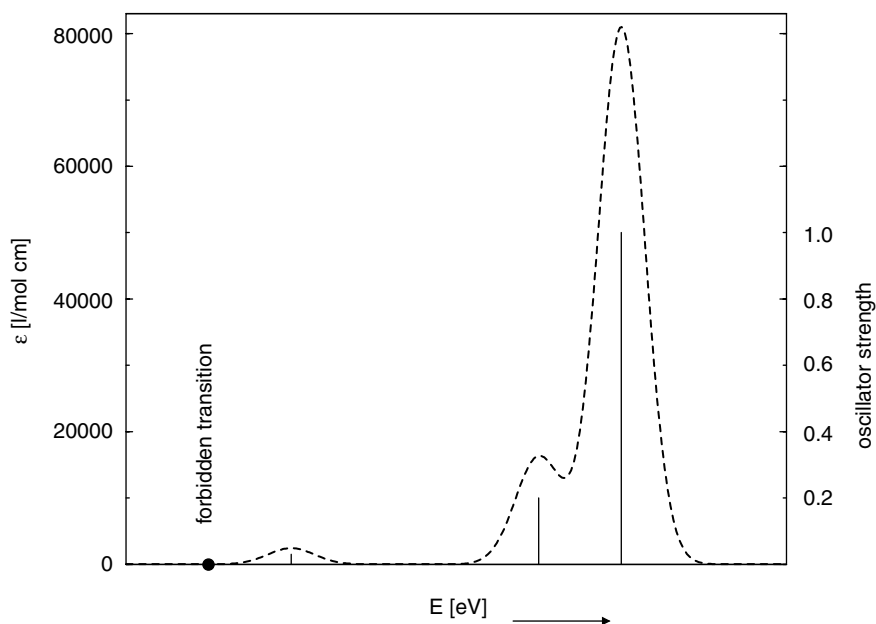


Figure 5 Example of the graphical presentation of a simulated (vertical) UV spectrum.

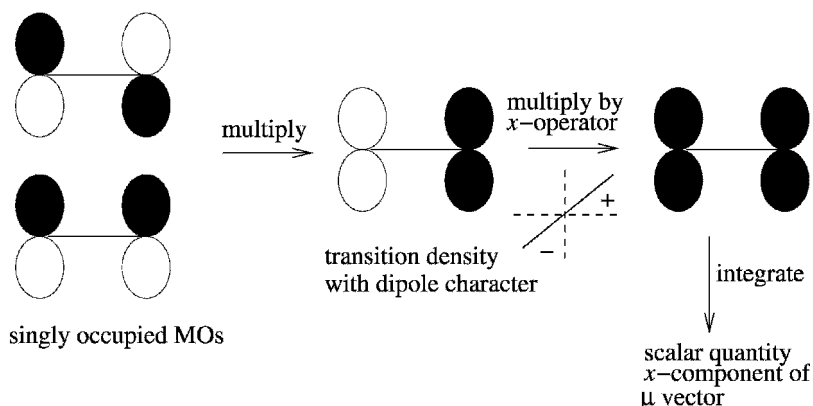


Figure 6 Schematic description for the process of generating the electric transition dipole moment for the  $\pi \rightarrow \pi^*$  excitation of ethene. Transparent (black) areas correspond to a positive (negative) phase.

For an electric dipole allowed transition, the radiation field must create or destroy a node in the corresponding transition density. A simple example is an atomic  $s \rightarrow p$  excitation, where the transition density is simply given by the product  $s \times p$ , which yields a scalar quantity when multiplied by  $r$  and integrated over space. In other words, the transition density must have a dipolar structure, where “probability” is shifted from positive-to-negative (and vice versa) regions. The mathematical process of generating the electric dipole transition moments is schematically outlined for the example of the  $\pi \rightarrow \pi^*$  transition of ethene in Figure 6.

If the transition density simultaneously has some rotational character, the magnetic component of the radiation field becomes important. For noncircularly polarized light, that is, in conventional UV spectroscopy, the magnetic component of the radiation field can be neglected in the time-dependent perturbation because it enters with a factor  $v_{\text{el}}^{\text{av}}/c$ ; the average electron velocity is much smaller than the speed of light. The effect of the magnetic component in circularly polarized light is observed experimentally in electronic circular dichroism (CD) spectroscopy of chiral molecules.<sup>43</sup> As a conventional absorption, it is a first-order, linear effect but depends on the combined interaction of a molecule with the electric and magnetic components of the radiation field.

The main quantity in CD is the rotatory strength  $R$ , which is completely analogous to the oscillator strength in UV spectroscopy and is given by the scalar product<sup>44,45</sup>

$$\begin{aligned}
 R_{nm} &= \text{Im} \langle \Psi_n | \hat{\boldsymbol{\mu}} | \Psi_m \rangle \times \langle \Psi_n | \hat{\boldsymbol{m}} | \Psi_m \rangle \\
 &= |\boldsymbol{\mu}_{nm}| \cdot |\boldsymbol{m}_{nm}| \cdot \cos(\boldsymbol{\mu}_{nm}, \boldsymbol{m}_{nm})
 \end{aligned}
 \tag{14}$$

where  $\hat{m}$  is the magnetic dipole operator (angular momentum)

$$\hat{m} = \frac{\hbar e}{2mci} \sum_k^{N_{el}} \hat{\mathbf{r}}_k \times \hat{\mathbf{v}}_k \quad [15]$$

In oriented media (which will not be considered here), additional dipole–quadrupole terms contribute to the CD. The rotatory strength is zero by symmetry if the molecule possesses at least one improper  $S_n$  axis as symmetry element (this causes either  $\mu$  or  $m$  to be zero or an orthogonal arrangement of the two vectors, see Eq. [14]). Also, in complete analogy to UV spectra,  $R$  can be obtained from Eq. [12] with  $\varepsilon$  replaced by the difference of extinction coefficients for left- and right-circularly polarized light ( $\Delta\varepsilon = \varepsilon_L - \varepsilon_R$ ).

The main perspective of CD spectroscopy is its potential to determine the absolute configurations of chiral substances that is of particular importance for compounds with biological or pharmacological relevance, for example. Furthermore, unlike optical spectra, the CD bands can be positive or negative, and for this reason carry more information and sometimes allow one to resolve close-lying or hidden electronic transitions. More details about theoretical CD spectroscopy can be found in Refs. 43 and 46–48. In Ref. 49 the CD spectra of a benchmark set of molecules have been investigated with the most recent quantum chemical methods. Some representative examples are discussed in a later section of this chapter. Recent advances in the theoretical description of magnetically induced CD, which in addition employs a static magnetic field, can be found in Ref. 50.

## Vibrational Structure

In general, the intensity  $I$  of a transition between the two states  $\Psi_m$  and  $\Psi_n$  is proportional to the square of the transition dipole moment

$$\boldsymbol{\mu}_{n,m} = \langle \Psi_n | \hat{\boldsymbol{\mu}} | \Psi_m \rangle \quad [16]$$

with the dipole operator

$$\hat{\boldsymbol{\mu}} = -e \sum_i \hat{\mathbf{r}}_i + e \sum_s Z_s \hat{\mathbf{R}}_s = \hat{\boldsymbol{\mu}}_e + \hat{\boldsymbol{\mu}}_N \quad [17]$$

where  $\hat{\mathbf{r}}_i$  and  $\hat{\mathbf{R}}_s$  denote the electron and nuclear coordinates, respectively, and  $Z_s$  represents the nuclear charges.

For the description of a vibronic transition both electronic and nuclear coordinates must be taken into account. In the adiabatic BO approximation, the complete wave function can be separated into the product

$$\Psi(\mathbf{r}, \mathbf{R}) = \Psi_e(\mathbf{r}; \mathbf{R}) \Psi_N(\mathbf{R}) \quad [18]$$

where  $\Psi_\varepsilon(\mathbf{r}; \mathbf{R})$  and  $\Psi_N(\mathbf{R})$  denote the electronic and nuclear wave functions, respectively (for a good review about treatments beyond the BO approximation see Ref. 51).

After the separation of translational, rotational, and vibrational modes of nuclear motion

$$\Psi_N(\mathbf{R}) = \Psi_t(\mathbf{R}_t)\Psi_r(\mathbf{R}_r)\Psi_v(\mathbf{R}_v) \quad [19]$$

the vibrational modes can be represented within the harmonic approximation as a product of eigenfunctions of the harmonic oscillator  $v_i(Q_i)$

$$\Psi_v(\mathbf{R}_v) = v(\mathbf{Q}) = v_1(Q_1)v_2(Q_2)\cdots v_N(Q_N) \quad [20]$$

where  $Q_i$  denote the vibrational normal coordinates. For the transition dipole moment  $\boldsymbol{\mu}_{\varepsilon'v',\varepsilon v}$  of a vibronic transition  $\varepsilon v \rightarrow \varepsilon' v'$  with quantum numbers  $\varepsilon$  and  $\varepsilon'$  for the electronic and  $v$  and  $v'$  for the vibrational parts of the initial and final state, respectively, these expressions give<sup>39</sup>

$$\boldsymbol{\mu}_{\varepsilon'v',\varepsilon v} = \langle v'(\mathbf{Q}') | \boldsymbol{\mu}_{\varepsilon',\varepsilon}(\mathbf{Q}) | v(\mathbf{Q}) \rangle \quad [21]$$

where  $v(\mathbf{Q})$  and  $v'(\mathbf{Q}')$  are the vibrational functions,  $\mathbf{Q}$  and  $\mathbf{Q}'$  are the normal modes of the initial and final states, respectively, and  $\boldsymbol{\mu}_{\varepsilon',\varepsilon}(\mathbf{Q})$  denotes the electronic transition dipole moment as a function of the initial state normal modes. Because for the transition dipole moment in general no analytical expression is available, it is expanded in a Taylor series around the initial state minimum geometry  $\mathbf{Q}_0$ .

$$\boldsymbol{\mu}_{\varepsilon',\varepsilon}(\mathbf{Q}) \approx \boldsymbol{\mu}_{\varepsilon',\varepsilon}(\mathbf{Q}_0) + \sum_i \frac{\partial \boldsymbol{\mu}_{\varepsilon',\varepsilon}}{\partial Q_i} (Q_i - Q_{i,0}) + \cdots \quad [22]$$

Truncation of the expansion after the first term yields the Franck–Condon (FC) approximation for the transition dipole moment

$$\boldsymbol{\mu}_{\varepsilon'v',\varepsilon v} = \boldsymbol{\mu}_{\varepsilon',\varepsilon}(\mathbf{Q}_0) \langle v'(\mathbf{Q}') | v(\mathbf{Q}) \rangle \quad [23]$$

In the FC picture, the transition occurs from the vibrational ground state of the initial electronic state to the vibrational excited state of the electronically excited state (considered in the following absorption), which most resembles the first one.<sup>52–54</sup> This is shown schematically in Figure 7 for two excited states that (with respect to the ground state) are shifted differently along one vibrational normal coordinate  $Q$ .

A description of electric dipole forbidden transitions, where  $\boldsymbol{\mu}_{\varepsilon',\varepsilon}(\mathbf{Q}_0) = 0$  is not possible in terms of the FC approximation, because vibronically induced

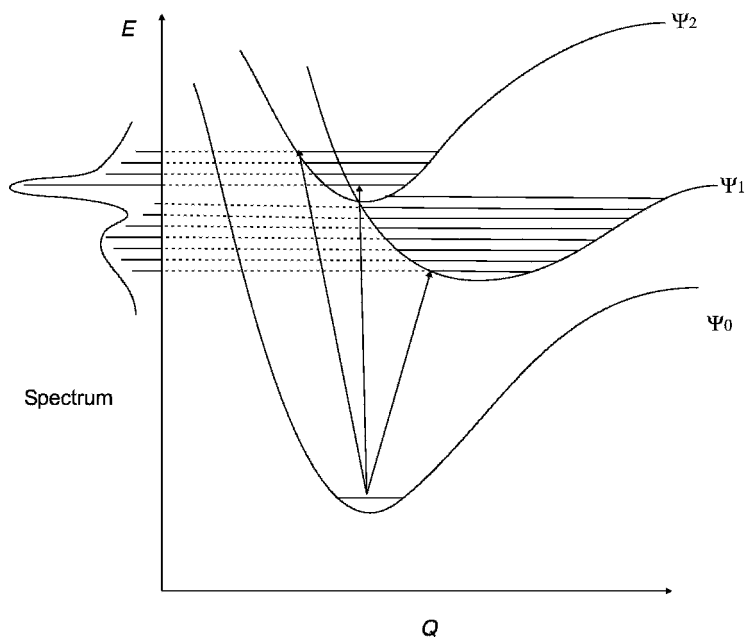


**Figure 7** Schematic description of the FC principle for two excited states with dominating 0–0 transition ( $\Psi_2$ , almost parallel potential surfaces) and a broad intensity distribution ( $\Psi_1$ , shifted minimum), respectively. The nonzero intensities for 0–1, 0–2, ... vibrational transitions to  $\Psi_2$  result entirely from the different shapes of the surfaces, while the intensity distribution for the other transition originates mainly from the shifted minimum.

transition moments are neglected. Truncation of the Taylor expansion (Eq. [22]) after the second term yields the Franck–Condon–Herzberg–Teller (FC–HT) approximation for the transition dipole moment

$$\mu_{\epsilon'\nu',\epsilon\nu} = \mu_{\epsilon',\epsilon}(\mathbf{Q}_0) \langle v'(\mathbf{Q}') | v(\mathbf{Q}) \rangle + \sum_i \frac{\partial \mu_{\epsilon',\epsilon}}{\partial Q_i} \langle v'(\mathbf{Q}') | (Q_i - Q_{i,0}) | v(\mathbf{Q}) \rangle \quad [24]$$

This description accounts for transition dipole moments induced by displacements along the normal modes during the electronic transition, that is, a simultaneous excitation of vibrational modes. This approximation is also denoted as double-harmonic. For electric dipole forbidden transitions, the first term in Eq. [24] vanishes and the resulting expression is denoted as the Herzberg–Teller (HT) approximation.

$$\mu_{\epsilon'\nu',\epsilon\nu} = \sum_i \frac{\partial \mu_{\epsilon',\epsilon'}}{\partial Q_i} \langle v'(\mathbf{Q}') | (Q_i - Q_{i,0}) | v(\mathbf{Q}) \rangle \quad [25]$$

A physical explanation for the influence on the transition dipole moment of vibrational excitations that occur simultaneously to the electronic transition is that displacements along the normal modes result in a perturbation of the electron–nuclear interaction. Thereby a mixing of the excited-state electronic wave function with other excited-state wave functions occurs that leads to a mixing of the corresponding transition dipole moments<sup>39,55</sup> (“intensity borrowing” from dipole-allowed transitions). Because this process depends critically on the energy separation between the target and the mixing states, a good overall description of the electronic spectrum is necessary to obtain reliable HT transition moments.

For molecules with more than one internal degree of freedom the normal modes of the ground and excited state are not in general identical (Duschinsky effect). Thus, for the calculation of the multidimensional integrals in Eqs. [23]–[25] it is necessary to describe the excited-state normal modes on the basis of the ground state taking into account the different minimum geometries. This is achieved by the following linear transformation (Duschinsky-transformation)<sup>56</sup>

$$\mathbf{Q}' = \mathbf{J}\mathbf{Q} + \mathbf{K} \quad [26]$$

with  $\mathbf{K} = \mathbf{L}'^T \mathbf{M}^{1/2} \Delta \mathbf{R}$  and the Duschinsky-matrix  $\mathbf{J} = \mathbf{L}'^T \mathbf{L}$ , where  $\mathbf{L}$  and  $\mathbf{L}'$  denote the normal modes in mass-weighted Cartesian coordinates of the ground and excited state, respectively,  $\Delta \mathbf{R}$  the difference of the minimum geometries and  $\mathbf{M}$  the diagonal matrix of the atomic masses. This relationship is exact for normal modes that—in the common symmetry group of ground and excited states—do not span the same symmetry species as one of the rotations. For normal modes having the same symmetry as one of the rotations, so-called “axis switching effects” occur.<sup>57,58</sup> Nevertheless the Duschinsky-transformation has been proven to be a good approximation.

With the use of a recursive algorithm,<sup>59</sup> the resulting integrals  $\langle v'(\mathbf{J}\mathbf{Q} + \mathbf{K}) | v(\mathbf{Q}) \rangle$  are reduced to the integral over the vibrational ground state from which the  $\langle v'(\mathbf{J}\mathbf{Q} + \mathbf{K}) | \mathbf{Q}_i | v(\mathbf{Q}) \rangle$  terms can be derived as well.<sup>60</sup> A further technical issue concerns the calculation of the normal modes and frequencies of the ground and excited states. In all vibronic structure treatments we employ a numerical approach, where the second derivatives of the energy and the derivatives of the transition moments are calculated by finite differences from analytical gradients and the transition moments, respectively. This is done very efficiently in parallel using an extended version of the program SNF 2.2.1.<sup>61,62</sup> For the calculation of the FC and HT integrals and all required level combinations in a user-specified energy interval, the HOTFCHT 1.2<sup>60</sup> program is used.

## Quantum Chemical Methods

### General

Before continuing with an overview of existing quantum chemical approaches for computing the excited states of large molecules, it seems appropriate to first define a “wish list” of the properties these methods should provide. Generally desired properties that also apply to ground states (e.g., size-consistency, weak AO basis set dependence, systematic improvability, etc.) are not included in this list.

1. **Applicability:** The method should be able to treat arbitrary types of excited states (see Table 1, first column), especially highly excited ones, and those occurring in photochemical applications. Spectral simulations sometimes require the simultaneous description of 10–100 states.
2. **Accuracy:** Errors for excitation energies should be  $< 0.1$ – $0.2$  eV, transition moments should be accurate to within 20–30% and the sign (direction) of the moment should be correct.
3. **Properties:** All standard one-electron properties and transition moments as well as analytical nuclear gradients for geometry optimization should be available. The method should allow interpretation of the results within simple (e.g., MO) models.
4. **Human effort:** The method should be of “black-box” character including as few technical parameters as possible.
5. **Computational:** Memory and CPU requirements should not be significantly larger than for the corresponding ground-state calculation.

Unfortunately, none of the methods currently in use simultaneously fulfill all these requirements. The user’s choice is thus determined by a consideration of the assets and drawbacks of a particular method which, in relation to the type of electronic spectra/states, may change from one problem to the other. Figure 8 provides the reader with a comprehensive overview of existing quantum chemical methods for excited states.

One of the basic problems to consider in advance concerns the multireference character of the ground state and the importance of multiply excited configurations in the excited states. The choice depicted in Figure 8 distinguishes between single-reference CI or TD approaches on the left and multi-reference treatments on the right (MR-CC and quantum Monte Carlo treatments also shown on the right side are currently under intense development and included only for completeness). Both groups of methods have their own advantages and disadvantages. The MR methods are general in a sense that once a zeroth-order [reference,  $\Psi^{(0)}$ ] wave function has been built up, any type of excited state can be treated. The price to pay, however, is that the choice of  $\Psi^{(0)}$  is not unique and furthermore requires a lot of human effort. In contrast, the starting point for the TD approaches is the electronic ground state, where the excitation energies (transition moments) are obtained as poles

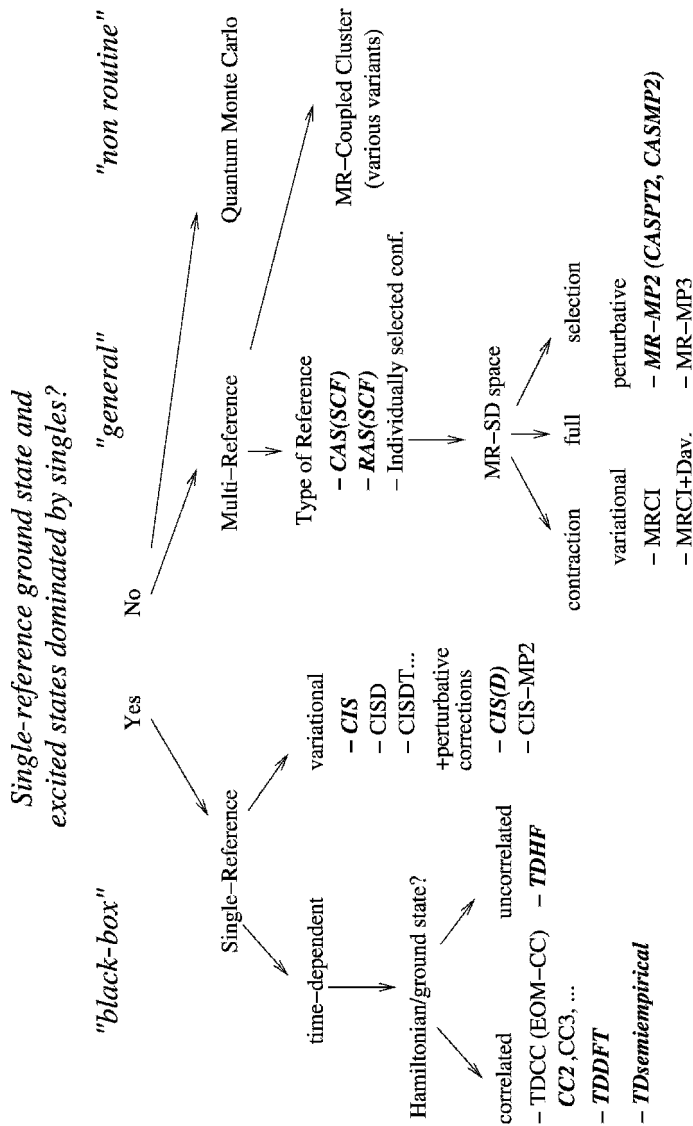


**Figure 8** An overview of quantum chemical methods for excited states. Bold-italic entries indicate methods that are currently applicable to large molecules. Important abbreviations used: CI (configuration interaction), TD (time-dependent), CC (coupled-cluster), HF (Hartree-Fock), CAS (complete active space), RAS (restricted active space), MP (Møller-Plesset perturbation theory), S (singles excitation), SD (singles and doubles excitation), MR (multireference). Geometry optimizations of excited states for larger molecules are now possible with CIS, CASSCF, CC2, and TDDFT methods.

(residuals) of the response of the ground state to a time-dependent perturbation (electric field).

The basic theoretical background of the most widely used methods will be outlined in the following sections including the most important working equations and technical issues that must be considered in large-scale applications.

### CI Methods

Although the application of configuration interaction (CI) methods to excited-state problems has decreased in recent years, they should be considered here first because the formalism is easy to understand and if properly developed, are also most general in application. A recent comprehensive review can be found in Ref. 63.

All CI methods are variational, that is, the electronic Schrödinger equation

$$\hat{H}|\Psi_n^{\text{CI}}\rangle = E_n^{\text{CI}}|\Psi_n^{\text{CI}}\rangle \quad [27]$$

is solved for state  $n$  with the following ansatz for the wave function

$$|\Psi_n^{\text{CI}}\rangle = (\hat{T}_1 + \hat{T}_2 + \hat{T}_3 + \dots)|\Psi^{(0)}\rangle \quad [28]$$

where  $\Psi^{(0)}$  is a so-called reference wave function and  $\hat{T}_k$  are the single (one-electron,  $k = 1$ ), double (two-electron,  $k = 2$ ) and triple (three-electron,  $k = 3$ ) excitation (replacement) operators, respectively. By acting onto  $\Psi^{(0)}$  these operators generate complete sets of (excited) determinants by substitutions of occupied orbitals  $i, j, k, \dots$  in the determinants of  $\Psi^{(0)}$  with virtual orbitals  $b, c, d, \dots$ . Note that in general, open-shell determinants are not eigenfunctions of the  $\hat{S}^2$  operator (they cannot be classified according to multiplicity as, e.g., singlet, doublet, triplet, ...). Actual treatments are often based on so-called configuration-state functions (CSF), which are represented by appropriate linear combinations of several determinants with the same  $M_s$  value (the term “configuration”, which is often used to characterize the spatial distribution of the electrons in the different orbitals, is merely used linguistically but cannot be employed in actual computations).

The most important contributions from singles and doubles excitation are given, for example, by

$$\hat{T}_1 = \sum_{ib} t_i^b a_i a_b^\dagger \quad [29]$$

$$\hat{T}_2 = \frac{1}{4} \sum_{ibjc} t_{ij}^{bc} a_i a_b^\dagger a_j a_c^\dagger \quad [30]$$

where  $t$  represent the unknown amplitudes (CI coefficients) and  $a$  and  $a^\dagger$  are the annihilation and creation operators, respectively. If  $\Psi^{(0)}$  is taken as a single determinant (usually the HF ground state), this leads to single-reference CI methods. Depending on the level of truncation of the excitation operator in Eq. [28], one obtains CIS (includes only  $\hat{T}_1$ ), CISD ( $\hat{T}_1 + \hat{T}_2$ ), CISDT, and so on, models. Of these, only CIS is widely used to calculate electronic spectra:

- The computational cost for CIS is similar to that of the ground-state HF calculation and can also be performed directly in the AO basis thus minimizing hard-disk I/O. The accuracy of CIS for excited states is roughly that of HF for the ground state, that is, dynamic electron correlation effects are neglected (for ground and excited states).
- The CISD provides an unbalanced description for the excited states relative to the ground state, because for a closed-shell ground state, the most important double excitations (which mainly account for EC) are included. On the contrary, an excited state, which is already singly excited with respect to the ground state, requires at least the inclusion of triple excitations (triples are related to the singles as the doubles are to the HF state). Thus, CISD grossly overestimates the excitation energies.<sup>64</sup> Note that this does not hold for LR-CCSD, which accounts for higher excitations by the exponential of the excitation operator. Compared to CIS, all other CI schemes are not size-consistent (i.e., the calculated excitation energy for two noninteracting fragments is not exactly the same as for separate calculations on the individual monomers).

There are two major routes to improve the CI methods. The first is by including size-consistent corrections for dynamical EC leading to the CIS(D) and CIS-MP2 methods<sup>65</sup> (which are closely related to the coupled-cluster methods described in a later section). The second is by improving the reference wave functions, which leads to multireference CI (MRCI) methods, that, however, remain size-inconsistent.

In the MRCI approach, one tries to reach a balanced description by setting up a zeroth-order wave function  $\Psi_n^{(0)}$  for each state of interest that includes the most important electronic configurations (static EC). For one particular state, then,

$$|\Psi_{\text{MR}}^{(0)}\rangle = \sum_a^{\text{references}} c_a^{(0)} |\Phi_a^{(0)}\rangle \quad [31]$$

where  $\Phi_a^{(0)}$  represent electronic configurations (determinants) with variationally determined coefficients  $c_a^{(0)}$ . A wide variety of different choices for  $\Psi_{\text{MR}}^{(0)}$  are currently in use, including full-CI within a selected set of orbitals (CAS), excitation restricted CI within a selected set of orbitals (RAS), or even individually (iteratively) selected configurations.

Application of this ansatz together with the truncation to single and double excitations as before (Eq. [28]) now includes all important contributions in a balanced manner. Hence, for a singly excited state, important parts of the triple excitations are included. The MR(SD)CI (the SD term is usually discarded in the abbreviation) method is very accurate for small- and medium-sized systems when the remaining size-consistency errors are corrected empirically, for example, via the Davidson scheme. Unfortunately, it is computationally very demanding to have an  $N_{\text{el}}^6$  scaling behavior with system size and a very large prefactor. It can be routinely applied only to systems with  $\sim 20$ – $40$  electrons (for benchmark or calibration DFT purposes). For a more efficient approach that empirically combines DFT and MRCI methods, and that can be applied also to large systems see Ref. 66, applications in electronic spectroscopy can be found in Refs. 67–71.

### Perturbation Methods

One way to retain the generality of the MR ansatz while reducing the computational costs is to use perturbation theory (PT). Perturbation theory has the important property of being size-consistent if properly formulated and implemented.<sup>72</sup> The starting point is again a reference wave function  $\Psi_n^{(0)}$  for a particular electronic state  $n$  that includes the most important contributions to the wave function. By construction,  $\Psi_n^{(0)}$  satisfies the eigenequation

$$\hat{H}_0|\Psi_n^{(0)}\rangle = E_n^{(0)}|\Psi_n^{(0)}\rangle \quad [32]$$

where  $\hat{H}_0$  is the zeroth-order Hamiltonian. In MP partitioning,  $\hat{H}_0$  is defined via the perturbation  $V$ , which is

$$\lambda \hat{V} = \hat{H} - \hat{H}_0 = \sum_i \sum_{j>i}^{N_{\text{el}}} 1/\hat{r}_{ij} - \langle \hat{V}_{ee} \rangle_{\text{average}} \quad [33]$$

the difference between the true and the mean-field (HF) electron–electron repulsion. In the MP schemes,  $\hat{H}_0$  is represented as a sum of general Fock operators that are state-dependent. As usual in perturbation theory, the energy and wave function are expanded in a Taylor series for  $\lambda$  that then leads to a (decoupled) system of linear equations for each perturbation order. For large systems, one usually truncates at second-order (for an approximate fourth-order treatment see Ref. 73) which leads to methods that scale as  $N_{\text{el}}^5$  with the system size. The second-order energy correction  $E^{(2)}$  is

$$E^{(2)} = - \sum_a t_a^{(1)} \langle \Phi_a^{(1)} | \hat{H} | \Psi_n^{(0)} \rangle \quad [34]$$

where  $\Phi_a^{(1)}$  is an element (CSF) of the first-order corrected wave function with amplitude  $t_a^{(1)}$  that is obtained by solving the linear equations

$$\sum_a t_a^{(1)} \langle \Phi_b^{(1)} | \hat{H}_0 - E_n^{(0)} | \Phi_a^{(1)} \rangle = -\langle \Phi_b^{(1)} | \hat{H} | \Psi_n^{(0)} \rangle \quad [35]$$

In general,  $\Psi^{(1)} = \sum_a t_a^{(1)} \Phi_a^{(1)}$  contains all single and double excitations from the reference that directly interacts through the true operator  $\hat{H}$  [the various variants of MRPT differ in how the annihilation and creation operators act on  $\Psi^{(0)}$ ].

A key point here is that in contrast to the MRCI case, the very large interaction matrix contains only elements between CSF and the simple one-electron operator  $\hat{H}_0$  (the costly interactions with  $\hat{H}$  appear only on the right side of Eq. [35] with the reference). This not only decreases the scaling behavior from  $N_{\text{el}}^6$  (CI) to  $N_{\text{el}}^5$  (PT), but also reduces the computational effort considerably because the one-electron matrix elements are very easy to evaluate. Apart from technical details for the solution of Eq. [35] (which especially holds for CASPT2, which uses a density matrix approach<sup>74</sup>), the different implementations of multireference perturbation theory (CASPT2,<sup>74–76</sup> CASMP2,<sup>77</sup> MR-MP2<sup>78</sup>) differ mainly by the choice of the reference wave function. Both CASPT2 and CASMP2 are based on complete-active-space wave functions as references that consist of a full CI treatment within an active space of orbitals–electrons and state-optimized orbitals while the MR-MP2 variant can employ arbitrary CI references and orbital sets. To be applicable for large molecules, careful consideration of technical details and implementation is necessary: There are at least two approaches<sup>76,78</sup> that have demonstrated good accuracy at reduced computational costs.

Within the “ab initio world”, CASPT2 became the de facto standard by chemists for the calculation of electronic spectra. Its first success was the accurate description of the electronic spectrum of benzene,<sup>75</sup> which at that time was a challenging goal for quantum chemistry. Since then, hundreds of applications of CASPT2 in electronic spectroscopy appeared that are described in existing reviews<sup>10–12</sup> (for the most recent application see Ref. [79]). The most severe drawback of CASPT2 is the full CI reference wave function on which it is based. Without symmetry, active spaces of 12 electrons in 12 orbitals in the preceding CASSCF treatment are the current limit that is often not enough for large unsaturated systems.

### *TDHF and TDDFT*

It is an understatement to say that DFT<sup>80,81</sup> has strongly influenced the evolution of quantum chemistry during the past 10–15 years. In the last 5 years, this statement also holds true for the treatment of excited states and, since then, time-dependent Kohn–Sham (KS) DFT (TDDFT)[82,83] has

become a routine tool to simulate electronic spectra. Both TDDFT and TDHF methods can be derived along similar lines as outlined briefly below.

We consider an  $N$ -electron system that is initially at time  $t = t_0$  in its ground state  $|\Psi_0\rangle$ . At times  $t > t_0$  a time-dependent perturbation  $\lambda\hat{U}(t)$  is applied. For our purposes, the most important perturbation is the electric dipole part ( $\boldsymbol{\mu}$ ) of a monochromatic radiation field given by

$$\hat{U}(t) = -\boldsymbol{\mu}Ee^{-i\omega t} \quad [36]$$

that oscillates with frequency  $\omega$  and has a (constant) field strength  $E$ . The linear response (LR) [index (1)] of an observable  $O(t)$  is defined as the first variation of the expectation value with respect to the scalar variable  $\lambda$

$$O^{(1)}(t) = \delta\langle\Psi(t)|\hat{O}(t)|\Psi(t)\rangle = \frac{d}{d\lambda}\langle\Psi(t)|\hat{O}(t)|\Psi(t)\rangle|_{\lambda=0} \quad [37]$$

where  $\Psi(t)$  is the time-dependent (ground-state) wave function. Graphically, we can imagine that  $\Psi(t)$  can be represented by the complete set of all excited eigenstates (including  $\Psi_0$ ) of the Hamiltonian and, thus, one can derive information about the desired excited states by considering the time evolution of  $\Psi(t)$ . More precisely, at certain frequencies  $\omega$  electronic transitions are stimulated and the first-order response of the ground state must diverge. For these values of  $\omega$ , the first-order response equations are exactly satisfied even if  $\boldsymbol{\mu}E$  is zero, since these are intrinsic molecular properties corresponding to free oscillations. In other words, solving the TD equations for some Hamiltonian with a particular ansatz for the ground-state wave function is equivalent to finding the poles of the frequency-dependent polarizability  $\alpha(\omega)$  (see Figure 9) that is given by the sum-over-states formula

$$\alpha(\omega) = \sum_n^{\text{all excited states}} \frac{f_{0n}}{\omega_n^2 - \omega^2} \quad [38]$$

The transition moment can be obtained as the residue given by

$$\langle\Psi_0|\boldsymbol{\mu}|\Psi_n\rangle = \lim_{\omega \rightarrow \omega_n} (\omega - \omega_n)\alpha(\omega) \quad [39]$$

Both the DFT and HF methods use an effective, one-particle (mean-field) Fock operator  $F$ . In general, it can be written as a functional of the first-order density matrix  $\gamma$  (see Eq. [8] with  $m = n = 0$ ) as

$$F[\gamma](t) = h[\gamma](t) + v_H[\gamma](t) - v_{xc}[\gamma](t) + \lambda U(t) \quad [40]$$

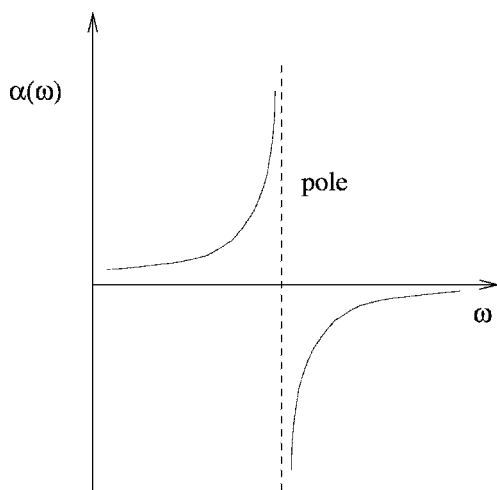


**Figure 9** Frequency dependence of the electric dipole polarizability  $\alpha(\omega)$ . The position of the dashed line corresponds to the system's excitation energy.

where  $h$  is the one-electron part of the Hamiltonian, the index  $H$  indicates the e-e Coulomb (Hartree) part and  $v_{xc}$  is a general (non-local, HF + local, DFT) exchange-correlation potential. In analogy to Eq. [37], the linear response of the mean-field (KS or HF) density matrix is

$$\gamma^{(1)}(t) = \frac{d}{d\lambda} \gamma(t)|_{\lambda=0} \quad [41]$$

By a Fourier transformation to the frequency domain, one obtains after expansion in the complete set of KS or HF one-particle eigenstates the following expression:

$$\gamma^{(1)}(\omega) = \sum_i \sum_a \left( \frac{u_{ai}(\omega)}{\omega - (\epsilon_a - \epsilon_i)} |i\rangle\langle a| \right) - \left( \frac{u_{ai}^*(\omega)}{\omega + (\epsilon_a - \epsilon_i)} |a\rangle\langle i| \right) \quad [42]$$

where  $i$  and  $a$  are occupied and virtual orbitals, respectively,  $\epsilon$  are their energies and  $u_{ai}$  are the matrix elements of the perturbation in the basis of the orbitals. Combining Eqs. [40] and [42] leads, after some algebraic manipulations, to a non-Hermitian eigenvalue problem that has to be solved for  $\omega = \Delta E$ . It is of the form

$$\begin{pmatrix} \mathbf{A} & \mathbf{B} \\ \mathbf{B} & \mathbf{A} \end{pmatrix} \begin{pmatrix} \mathbf{X} \\ \mathbf{Y} \end{pmatrix} = \Delta E \begin{pmatrix} 1 & 0 \\ 0 & -1 \end{pmatrix} \begin{pmatrix} \mathbf{X} \\ \mathbf{Y} \end{pmatrix} \quad [43]$$

where  $\mathbf{X}$  and  $\mathbf{Y}$  are the solution vectors of the single particle-hole (excitations,  $|i\rangle\langle a|$ ) and hole-particle (deexcitation,  $|a\rangle\langle i|$ ) amplitudes, respectively, and  $\mathbf{A}$ ,  $\mathbf{B}$  are related to Hamiltonian matrices between the single (de)excitations that are made from one-particle eigenvalues and Coulomb and exchange integrals over the MOs.<sup>84,85</sup> If formulated in the AO basis, Eq. [43] can be solved efficiently with computational effort similar to that of the preceding ground-state SCF calculation. If the matrix  $\mathbf{B}$  is set to zero, Eq. [43] reduces to a normal eigenvalue problem including only single excitations ( $\mathbf{Y} = \mathbf{0}$ , CIS). For DFT variants of CIS, see Refs. 86 and 87. An important advantage of TDHF(DFT) over CIS is that the former methods satisfy, in a complete AO basis, certain sum-rules, for example,  $\sum_i^\infty f_i = N_{\text{el}}$ .

The actual form of the mean-field applied to the ground state (HF or Kohn–Sham DFT) determines the explicit expressions for the matrix elements. In a general notation including TDHF as well as TDDFT, they read

$$A_{ia\sigma,jb\tau} = \delta_{\sigma\tau}\delta_{ij}\delta_{ab}(\varepsilon_{a\sigma} - \varepsilon_{i\tau}) + (i_\sigma a_\sigma | j_\tau b_\tau) - \delta_{\sigma\tau} c_{\text{HF}}(i_\sigma j_\sigma | a_\tau b_\tau) \quad [44]$$

$$B_{ia\sigma,jb\tau} = (i_\sigma a_\sigma | b_\tau j_\tau) - \delta_{\sigma\tau} c_{\text{HF}}(i_\sigma b_\sigma | a_\tau j_\tau) + (1 - c_{\text{HF}})(i_\sigma a_\sigma | f_{\sigma\tau} | b_\tau j_\tau) \quad [45]$$

where  $i, j$  are used for ground-state occupied orbitals,  $a, b$  for virtual orbitals, and  $\sigma$  and  $\tau$  are the spin variables. The parameter  $c_{\text{HF}}$  is the coefficient of the “exact” HF exchange (EEX) part in hybrid functionals. Thus, similar to the ground state, there is a continuous change from TDHF to TDDFT when hybrid functionals with a variable amount of HF exchange contribution are considered. A lot of numerical evidence indicates that this also holds for calculated properties of ground and excited states.

The last terms in these equations, which are of DFT origin, are defined as

$$(i_\sigma a_\sigma | f_{\sigma\tau} | j_\tau b_\tau) = \iint i(r_1) a(r_1) f_{\sigma\tau}^{xc}(r_1, r_2) j(r_2) b(r_2) dr_1 dr_2 \quad [46]$$

In the so-called adiabatic approximation, the time-dependent exchange-correlation kernel  $f^{xc}$  is derived from the time-independent ground-state functional,

$$f_{\sigma\tau}^{xc}(r_1, r_2) = \frac{\delta^2 E_{xc}}{\delta\rho_\sigma(r_1)\delta\rho_\tau(r_2)} \quad [47]$$

This approximation should work best for  $\omega \rightarrow 0$ , that is for energetically low-lying excited states.

The magnitude of the excitation energies is determined mainly by the diagonal part of the matrix  $\mathbf{A}$ . For the closed-shell case, one obtains as a

zeroth-order approximation for the excitation energy of a state represented by a single substitution between MOs  $i$  and  $b$

$$\Delta E = \varepsilon_b - \varepsilon_i - c_{\text{HF}}(ii|bb) - (1 - c_{\text{HF}})(ii|f|bb) + 2(ib|ib) \quad [48]$$

Although this is often quantitatively a drastic approximation (due to the neglect of configuration mixing), a closer inspection of Eq. [48] gives some insight into the factors that determine excitation energies. In the HF case ( $c_{\text{HF}} = 1$ ), the difference of orbital energies is a very crude approximation because the Coulomb integral  $(ii|bb)$  represents a significant correction, that is, lowering of the excitation energy [the exchange integrals  $(ib|ib)$  are usually one order of magnitude smaller]. This is different in DFT, where the  $\Delta\varepsilon$  term is much smaller and where the Coulomb interaction is replaced by a response integral containing the (local) exchange-correlation kernel. This locality of the DF leads to severe problems when the excitation is connected with a spatial separation of the hole-particle as for Rydberg or charge-transfer states. For a very early attempt to correct this in the DFT/SCI(CIS) methods, see Ref. 86. Consider, for example, a charge-transfer excitation from donor orbital  $i$  to the acceptor orbital  $b$  [where  $(ib|ib) \approx 0$ ]. One obtains

$$\Delta E = \text{IP} + \text{EA} - c_{\text{HF}}(ii|bb) - (1 - c_{\text{HF}})(ii|f|bb) \quad [49]$$

where we have approximated the ionization potential IP by  $\varepsilon_i$  and the electron affinity EA by  $\varepsilon_b$ . The interaction between the separated charges must be described by the Coulomb law, that is,  $c_{\text{HF}}(ii|bb) + (1 - c_{\text{HF}})(ii|f|bb) \propto 1/R$ , where  $R$  is the distance between the hole-particle. Because  $c_{\text{HF}} = 0$  for pure DF and  $(ii|f|bb)$  falls off exponentially, the  $1/R$  fall-off condition is not fulfilled. This analysis shows that the inclusion of nonlocal HF exchange  $c_{\text{HF}} > 0$  in a local (pure) density functional is essential to describe charge- and spin-separating situations.

### *Coupled-Cluster Methods*

The basic idea of most coupled-cluster (CC) approaches for excited states is the same as for the TDHF/DFT methods: Excitation energies are obtained as the poles (where, e.g., the frequency-dependent polarizability goes to infinity) of the ground-state response with respect to a time-dependent perturbation. The important difference is that the ground state is not described by a single HF/KS determinant but (similar to the CI ansatz) by many singly, doubly, and so on, substituted configurations. The important size-consistency property is included in the CC methods by using the exponential of the excitation operator

$$|\Psi_{\text{CC}}\rangle = e^{\hat{T}}|\Psi^{(0)}\rangle \quad [50]$$

By choosing  $|\Psi^{(0)}\rangle \neq \Psi_{\text{HF}}$ , one arrives at MR-CC methods that are currently an active field of research, but that are not applied routinely except for benchmark systems. Similar to the CI method, truncation of the excitation operator then leads to a hierarchy of methods termed CCS (which is equivalent to CIS for energies), CCSD, CCSDT, and so on.

Applying the time-dependent perturbation is straightforward and leads to LR-CC methods. The nonlinear systems of equations include the “normal”  $T_1$  and  $T_2$  (for CCSD) operators—amplitudes and additionally single and double excitation (time-dependent) response amplitudes (for details the reader is referred to Refs. 1, 64, 88, 89 and references cited therein). An alternative approach, that, although conceptually different yields exactly the same excitation energies, is the equation-of-motion coupled cluster (EOM-CC) method [90]. The EOM-CC equations also contain the CC wave function  $|\Psi_{\text{CC}}\rangle$  (Eq. [50]) and a second (state-dependent) excitation operator  $\hat{R}_n$  including single, double, . . . excitations (usually  $\hat{R}$  is truncated in the same manner as  $\hat{T}$ ). The EOM equations read as

$$[\hat{H}', \hat{R}_n]|\Psi_{\text{CC}}\rangle = \omega \hat{R}_n \Psi_{\text{CC}} \quad [51]$$

where  $\hat{H}' = \hat{H} - E_{\text{HF}}$ .

One characteristic of all LR/EOM-CC methods is that a non-Hermitian eigenvalue problem finally has to be solved (which cannot be reduced to a standard eigenvalue problem as Eq. [43]) yielding “left” and “right” sets of solutions, and therefore also two sets of transition moments.

A “break through” for the application of the CC methods to excited states of large systems has recently been obtained by Christiansen et al.<sup>91</sup> These authors introduced a simplified LR-CCSD method termed CC2, where the doubles excitation operator is taken from second-order perturbation theory ( $\hat{Q}_2$ ). The CC2 ground-state wave function can be written as

$$|\Psi_{\text{CC2}}\rangle = e^{\hat{T}_1 + \hat{Q}_2} |\Psi^{(0)}\rangle \quad [52]$$

and thus only the singles amplitudes remain as free parameters while the doubles contributions  $\hat{Q}_2$  are taken from a MP2 treatment, that is, from

$$q_{ij}^{ab} \approx \frac{\langle ia|jb\rangle}{(\varepsilon_a + \varepsilon_b - \varepsilon_i - \varepsilon_j)} \quad [53]$$

which reduces the scaling behavior from  $\mathcal{O}(\mathcal{N}_{\text{el}}^6)$  to  $\mathcal{O}(\mathcal{N}_{\text{el}}^5)$ . In general, CC2 excitation energies are only slightly inferior to those from full CCSD. A further reduction of the computational costs in CC2<sup>92</sup> has been obtained by using the resolution-of-the-identity (RI) approximation for the two-electron integrals. The very efficient RI method is also used here in MR-MP2 and MRCI

methods as described before [66, 78]. The error for the excitation energies introduced by the RI approach is  $\sim 0.01\text{--}0.03$  eV, which is clearly insignificant compared to other sources of error like basis set truncation error that is of the order of  $0.1\text{--}0.2$  eV with standard cc-pVTZ basis sets. An analytical gradient for RI-CC2 has also been reported recently,<sup>93</sup> which routinely allows for geometry optimizations of medium-sized molecules. This recent advance includes a significant fraction of dynamical electron correlation (as opposed to CIS and CASSCF that have hitherto been frequently used for that purpose).

### *Recommendations*

Here, we provide a summary of the quantum chemical methods that can, and should be applied to the calculation of electronic spectra of large systems:

1. Hartree–Fock based methods (TDHF and CIS): Good energetic results from these methods cannot be obtained; the errors for excitation energies often exceed 0.5 eV. For low-spin states,  $\Delta E$  is often too large so scaling factors of  $\sim 0.7\text{--}0.8$  are in use while the  $\Delta E$  values for high-spin states are usually underestimated. Contrary to statements in the literature,<sup>94</sup> the results are often even qualitatively wrong (false state ordering). The Rydberg states, for which they appear to perform reasonably well, are not really important for large systems. Because excited-state geometries are relatively insensitive to correlation effects, these methods may be used (after careful calibration) for that purpose but even this is difficult because the predicted order of states is often wrong. Both TDHF and CIS methods have a tendency (as does HF for ground states) to break symmetry, and consequently they often yield geometries that are too distorted. They are to be preferred over TDDFT if the asymptotic behavior of the potential (see below) is of crucial importance. They are sometimes applicable if only relative trends in a series of very similar molecules are of interest.
2. Coupled-cluster methods: For systems with well-behaved ground states, and, if the excited states are reasonably described by single excitations, low-order coupled cluster methods (CC2<sup>91</sup> or LR/EOM-CCSD<sup>64, 90</sup>) can provide good accuracy (errors  $< 0.3$  eV). Especially when used together with efficient integral approximations (RI-CC2<sup>92</sup>) computations can be performed for fairly large molecules. For more complicated excited states or when the ground state is already strongly correlated, the inclusion of  $\hat{T}_3$  is mandatory, which limits the applicability to small molecules.
3. Perturbation methods: In general, second-order multireference PT methods can be recommended for excited-state problems. They usually show very good accuracy (errors  $< 0.2$  eV, excitation energies are systematically underestimated) and they can be applied to a wide variety of states and problems. However, MRPT methods are not “black-box” and careful checks of the technical details like the size of reference space, choice of orbitals, and so on, must be done. These methods require a lot of user

experience, as well as detailed insight into the system. For many states in the high-energy regions, the reference wave functions become prohibitively large, and, the second-order treatment often breaks down. The most serious disadvantage is that the results are very sensitive to the so-called “intruder states”, which have low zeroth-order energies but are only weakly interacting with the reference state.

4. Density functional methods: The TDDFT approaches employing hybrid functionals such as B3LYP<sup>20,21</sup> or BHLYP<sup>95</sup> are always the method of choice for providing a first overview about the electronic spectrum of a particular molecule. The errors for  $\Delta E$  are much smaller than with TDHF/CIS and usually within 0.3–0.4 eV of experiment (often  $\Delta E$  is underestimated). For larger transition metal compounds, TDDFT is the only method that is routinely applicable. The same holds for spectra, where on the order of a hundred different states must be considered. With common (asymptotically incorrect) functionals, larger errors are obtained for Rydberg<sup>85,96</sup> (see the following section) and charge-transfer states<sup>97–99</sup> or for states with strong contributions from ionic valence-bond structures.<sup>35</sup> A calibration on ab initio or experimental data and a check of the functional dependence of the results is strongly recommended.
5. Basis sets: The basis set requirements in excited-state applications are not very different than those for the corresponding ground state if only low-lying valence states are considered, and thus, properly polarized valence-triple- $\zeta$  (or even double- $\zeta$ ) sets are often good enough (i.e., they provide  $\Delta E$  to within 0.1 eV). Because the valence excited states of medium-sized systems can sometimes include diffuse components, a check of, for example, the  $\langle r^2 \rangle$  expectation values (see the following section) is recommended and depending on its value, diffuse basis functions must be added (for an example, see a later section). For low-lying Rydberg states, additional atom-centered diffuse sets of single- $\zeta$  quality ([1s1p1d]/[1s1p] for main group compounds) are sufficient.
6. Semiempirical approaches represent an alternative quantum chemical method especially for very large systems or when only main group compounds without complicated electronic structure are involved. As for the ground states, however, they are gradually being displaced by the more accurate and robust DFT methods. Of the many semiempirical approaches, the all-valence methods with orthogonalization corrections<sup>100,101</sup> and the simplest Pariser–Parr–Pople (PPP) type methods for very large  $\pi$ -systems can be recommended (for a recent application to a 600 atom system, see Ref. 102). One area of application is the prediction of excited-state geometries where MNDO/CI approaches seem to be quite successful.<sup>103,104</sup> For excitation energies, however, standard MNDO, AM1, or PM3 Hamiltonians employing small CI expansions show large systematic as well as unpredictable (random) errors. Careful calibration is thus mandatory with all semiempirical methods.

## CASE STUDIES

### Vertical Absorption Spectra

#### *Acetone*

In this section, some general aspects of the computation of Rydberg spectra are discussed (for reviews on this topic, see Ref. 6 and Ref. 105; for a recent theoretical study on very high-lying Rydberg states (which will not be considered here), see Ref. 106). Although Rydberg states are ubiquitous, they are of lesser importance in the spectra of large molecules that are dominated by valence states. The reason to begin this section with this topic is twofold: First, Rydberg states are mostly of relatively simple structure, being dominated by a few (mostly one) single excitations and are thus easy to understand intuitively in a MO picture. Second, the excitation process is accompanied with a spatial separation of the electrons that is typical also for some valence states. This leads to problems with most density functionals as already discussed in an earlier section.

The transitions to Rydberg states generally have low intensities because of the large spatial extension of the final orbital (small overlap with the origin orbital yields weak transition densities) and consequently they are often hidden under more intense valence bands. As an example, here we therefore have to investigate a small molecule where the valence transitions are spectrally separated. Saturated ketones show only two valence states, namely, the  $n \rightarrow \pi^*$  state at  $\sim 4$  eV and a very high-lying  $\pi \rightarrow \pi^*$  state so that a number of Rydberg transitions can be observed in the 6–9-eV range. Acetone, the simplest aliphatic ketone, is probably the best experimentally studied molecule of this group of important organic systems. Of the few theoretical studies that exist, we mention here only the most recent CASPT2 work of Merchan et al.,<sup>107</sup> where key references to the experimental data and older theoretical work can also be found.

Figure 10 shows the two orbitals that are involved in the first  $n \rightarrow 3s$  Rydberg transition of acetone. The very different spatial extensions are clearly visible and especially in the outer regions of the  $3s$  MO its almost spherical character can be seen.

The distinction between Rydberg and valence states is not that clear in larger molecules. A good indicator for the state character can be obtained from the  $\langle r^2 \rangle$  expectation value (a measure of spatial extension) difference for state  $n$  with respect to the ground state. This is given by

$$\Delta\langle r^2 \rangle = \langle \Psi_n | \hat{r}^2 | \Psi_n \rangle - \langle \Psi_0 | \hat{r}^2 | \Psi_0 \rangle \quad [54]$$

where

$$\hat{r}^2 = \hat{x}^2 + \hat{y}^2 + \hat{z}^2 \quad [55]$$

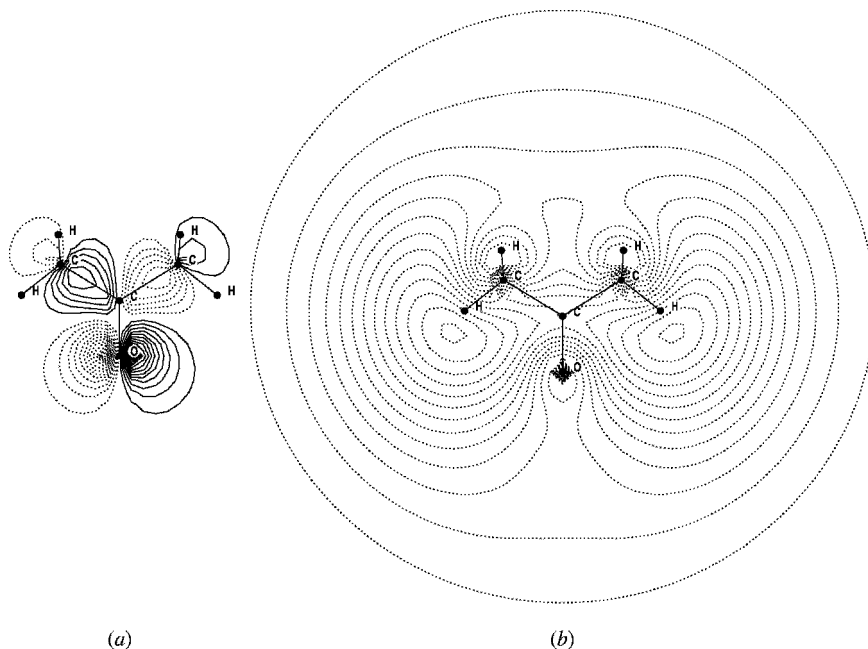


**Figure 10** Contour plots of the lone-pair MO (a) and 3s Rydberg MO (b) for acetone in the O–CCC plane. Because of the too high potential for the virtual orbitals in ground-state HF treatments, the calculations refer to a ROHF/d-aug-cc-pVDZ treatment for the  ${}^2B_2$  cation ground state.

is the trace of the Cartesian electric quadrupole operator. For molecules composed of second-row atoms, the  $\Delta\langle r^2 \rangle$  values are usually in the range 30–50 (3s), 50–100 (3p), and  $> 100 a_0^2$  for 3d states, respectively, while they are usually  $< 10 a_0^2$  for pure valence states.

The “diffuseness” of Rydberg states leads to complications with some quantum chemical approaches. When using MRCI or MRPT2 methods it is absolutely necessary to use virtual orbitals that are optimized in the presence of the correct potential of  $N_{\text{el}} - 1$  electrons. The (closed-shell) HF potential for the virtual orbitals includes the (nuclear charge) shielding of all  $N_{\text{el}}$  electrons and thus the Rydberg part of the spectrum is too diffuse, which leads to artificial configuration mixing in the CI procedures (to a lesser extent, however, this also holds for some valence states, especially for medium-sized systems). Experience shows that individually optimized orbitals are not necessary, but instead, ROHF orbitals of, for example, the lowest cation state, can be employed.

The problems of most density functionals with Rydberg states are also related to the electronic potential far away from the nuclei. It is well known that the local density approximation (LDA) exchange potential  $v_X^{\text{LDA}} \propto \rho(r)^{1/3}$

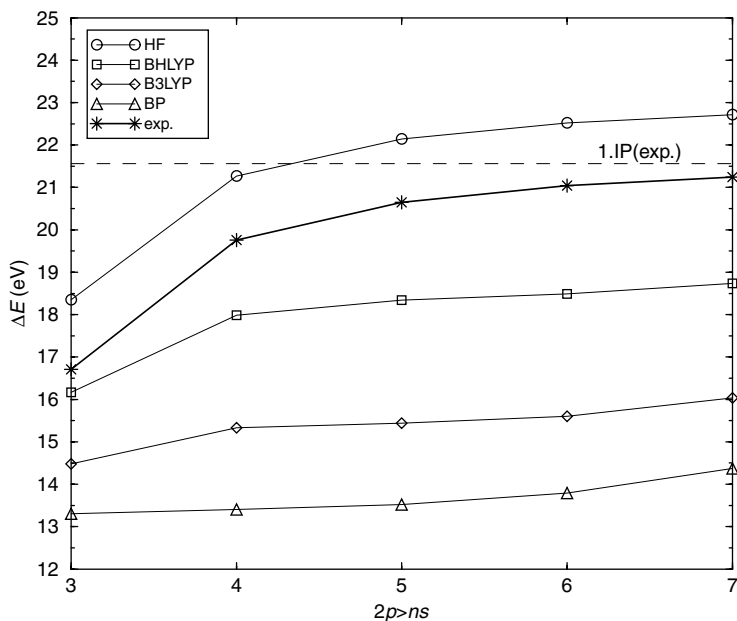


**Figure 11** Excitation energies for the singlet  $2p \rightarrow ns$  ( $n = 3-7$ ) Rydberg series of the neon atom ( $[6s4p] + 8s$  AO basis).

decays asymptotically exponentially with  $r$  [as the density  $\rho(r)$  itself] instead of with  $1/r + \text{const}$ . This behavior, which can also be explained by the artificial electron self-interaction, leads to (a) too small electron binding, that is, too low Rydberg excitation energies and to (b) a too fast approach of the asymptotic (ionized) limit. Figure 11 shows the  $\Delta E$  values for the  $2p \rightarrow ns$  ( $n = 3-7$ ,  $n$  indicates the principal quantum number) Rydberg series of the neon atom as calculated with TDHF and various TDDFT methods.

It is seen that while the TDHF results are just shifted with respect to the experimental data, the shape of the  $\Delta E$  versus  $n$  curves is qualitatively wrong with the TDDFT methods. With a pure DF completely lacking “exact” HF exchange (e.g., BP86<sup>108, 109</sup>) there is not only a large underestimation of the  $\Delta E$  values, but furthermore almost no dependence on  $n$  up to  $n = 6$  and after that even a strong energy increase is clearly visible. As expected, the situation is gradually improved by “exact” exchange mixing (from 20% in B3LYP to 50% in BHLYP<sup>95</sup>) and only the latter functional can be recommended for the computation of Rydberg spectra. The construction of a DF with the correct asymptotic behavior is currently an active field of research (for details and possible solutions to the problem see Refs. 96, 110, 111 and references cited therein).

This behavior of the DF is also observed in molecular applications. Vertical singlet excitation energies from CASPT2<sup>107</sup>, TDDFT-B3LYP, and

**Table 5.** Calculated and Experimental Excitation Energies (in eV) and Other Properties of the Vertical Singlet Excited States of Acetone

State	$\Delta E$				$f^L$	$\Delta\langle r^2 \rangle$
	B3LYP	CASPT2 <sup>a</sup>	MRCI	Exp. <sup>a</sup>		
$1B_2(n \rightarrow 3s)$	5.71	6.58	6.51	6.35	0.037	46.2
$2A_2(n \rightarrow 3p_x)$	6.61	7.34	7.41	7.36		75.7
$2A_1(n \rightarrow 3p_y)$	6.50	7.26	7.44	7.41	0.006	90.7
$2B_2(n \rightarrow 3p_z)$	6.66	7.48	7.49	7.45	0.002	85.6
$3A_1(n \rightarrow 3d_{yz})$	7.12	7.91	8.14	7.80	0.047	123.0
$3B_2(n \rightarrow 3d_{x^2-y^2})$	6.93	8.04	7.92	8.09	0.048	109.7
$3A_2(n \rightarrow 3d_{xz})$	7.24	8.09	8.17			118.0
$4B_2(n \rightarrow 3d_{z^2})$	7.18	8.18	8.21		0.004	133.3
$1B_1(n \rightarrow 3d_{xy})$	7.17	8.20	8.25	8.17	0.002	131.1

<sup>a</sup>Ref. 107.

MRCI computations (d-aug-cc-pVDZ AO basis, B3LYP/TZV(d,p) ground-state geometry) are compared with experimental data in Table 5. A graphical comparison with an experimental gas-phase absorption spectrum is shown in Figure 12.

The underestimation of the  $\Delta E$  values with TDDFT increases from  $\sim 0.65$  eV for the  $n \rightarrow 3s$  transition to  $> 1$  eV for the  $n \rightarrow 3d$  states. The

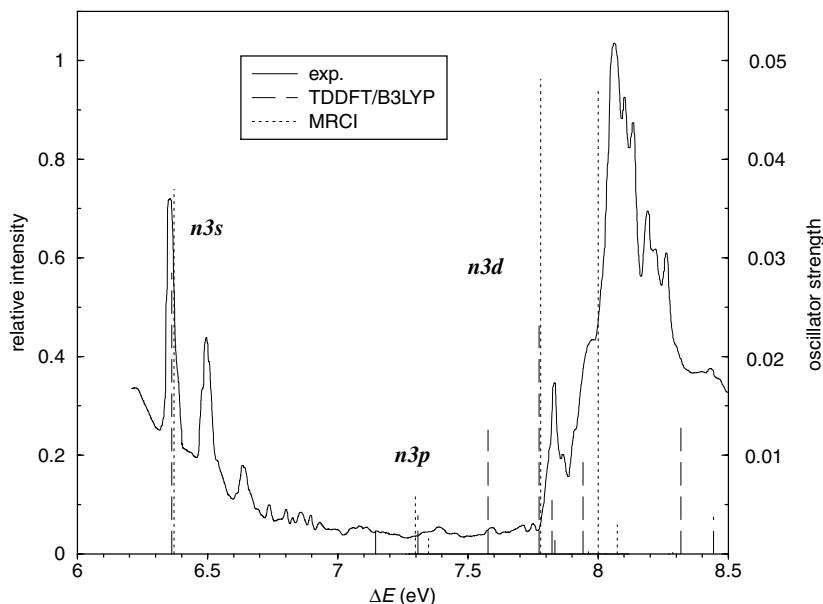


**Figure 12** Comparison of the experimental UV spectrum of acetone<sup>112</sup> with calculated vertical transitions. The theoretical  $\Delta E$  values are shifted by  $-0.15$  (MRCI) and  $0.65$  eV (TDDFT), respectively.

ab initio methods CASPT2 and MRCI uniformly provide a very accurate description of the spectrum with errors of  $\sim 0.1\text{--}0.2$  eV, which is on the order of the expected geometry relaxation effects. The largest error is found for the most core-penetrating  $3s$  state. Significant differences between CASPT2 and MRCI results are obtained for the order of the  $3p_x$  and  $3p_y$  states, where MRCI seems to be better. According to the MRCI results, the assignment of the  $3d_{yz}$  and  $3d_{x^2-y^2}$  has to be interchanged. As can be seen from Figure 12, the relative oscillator strengths compare quite well with the experimental intensities keeping in mind that geometry changes in the excited states are quite significant for acetone (cf. the potential curves in Ref. 107).

### *Organic Dyes*

Compounds that absorb in the range 380–720 nm are perceived as being colored, and, if the absorbance is strong they can be used as colorants.<sup>113</sup> Due to their industrial importance, there is continued interest in the theoretical prediction of the spectral properties of such compounds. While the computation of the lowest-lying (visible) bands in dyes is relatively straightforward due to the simple electronic structure of the corresponding excited states (mostly HOMO–LUMO single excitations), the higher-lying transitions are rarely considered. It is to be noted, however, that most  $\pi \rightarrow \pi^*$  excited states (even the simple HOMO–LUMO excited ones) have large dynamic EC contributions (mainly due to  $\sigma - \pi$  correlation), which must be considered in accurate work.

In this section, we consider, as examples, the UV spectra of two organic dyes: thioindigo and coumarin 102. We will use TDDFT, which today is the most successful and widely used method to calculate the electronic spectra of such compounds. Thioindigo belongs to the group of the indigoid dyes with one of the oldest known organic dyes, indigo, as a parent system. Thioindigo, in which both NH groups are replaced by sulfur, is a useful red vat dye and some of its halogenated derivatives are used as pigments.<sup>113</sup> Compounds based on the coumarin ring system give rise to one of the most extensively investigated and commercially important groups of organic fluorescent materials that are very well characterized for their use as laser dyes.<sup>114</sup> For other theoretical (DFT) work on coumarins, see Refs. 115–117.

The geometry optimizations for the ground-state structures of the investigated dyes as well as all TDDFT computations were carried out with the B3LYP functional and employed a TZV(d,p) AO basis set. The optimized ground-state structure of thioindigo has  $C_{2b}$  symmetry; coumarin is already nonplanar in the ground state due to slight pyramidalization of the  $NR_2$  group. A comparison between the experimental and calculated spectra of thioindigo and coumarin 102 is given in Figures 13 and 14, respectively. Note that in contrast to most of the other spectra presented in this work no energy shift has been applied meaning that the uncorrected TDDFT excitation energies already match the experimental (solution) data very closely.

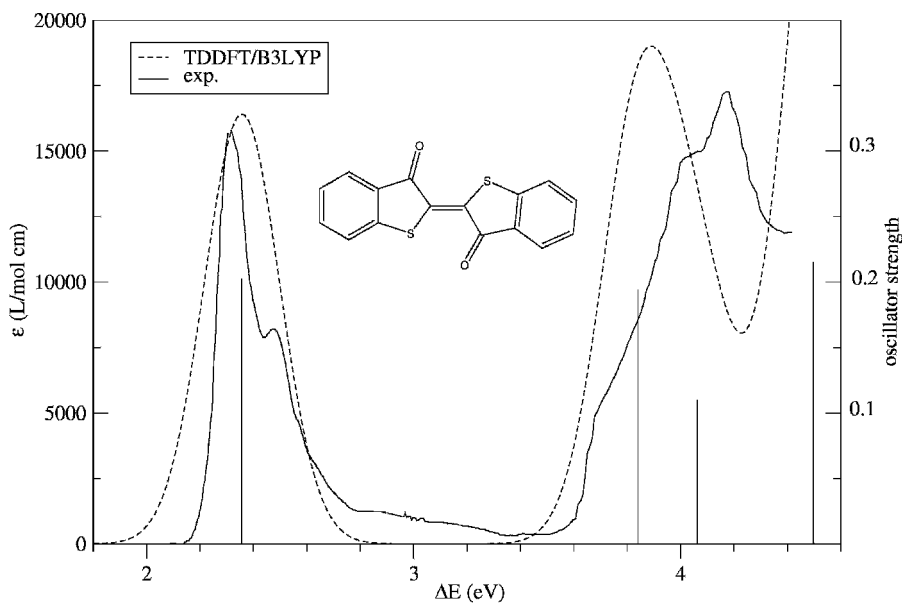


Figure 13 Comparison of experimental and computed [B3LYP/TZV(d,p)] UV spectra of thioindigo.

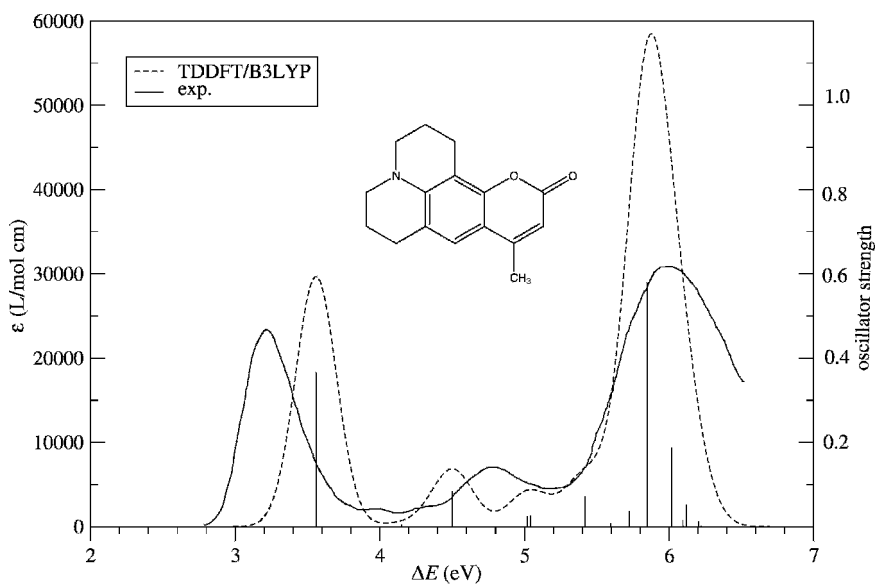


Figure 14 Comparison of experimental and computed [B3LYP/TZV(d,p)] UV spectra of coumarin 102.

The visible and near-UV spectrum of thioindigo measured in benzene show two major bands with maxima at  $\sim 2.3$  and  $4.2$  eV,<sup>118</sup> respectively. The calculated lowest excitation energy and oscillator strengths, which are arguably of most interest to the dye chemist, are in excellent agreement with the experimental values. The lowest lying  $1^1B_u$  state computed at  $2.36$  eV is of  $\pi \rightarrow \pi^*$  character and results mainly from the HOMO  $\rightarrow$  LUMO excitation. Despite this simple electronic structure, the (dynamical) EC contributions are large as can be seen by comparison with the TDHF excitation energy ( $3.77$  eV), which is in error by  $> 1.4$  eV. The second feature observed in the UV spectrum of thioindigo is a relatively broad absorption including two shoulders at  $3.7$  and  $4.1$  eV. Our calculations show that in this energy region there are two  $1^1B_u$  transitions close in energy: The  $2^1B_u$  computed at  $3.84$  eV and the  $3^1B_u$  at  $4.06$  eV. Both states have purely  $\pi \rightarrow \pi^*$  character and result mainly from HOMO-3 $\rightarrow$ LUMO and HOMO-6 $\rightarrow$ LUMO excitations, respectively. The almost perfect agreement between the experimental and calculated spectral data demonstrates that TDDFT provides a very reliable description of higher-lying valence states.

The experimental absorption spectrum of coumarin 102 obtained in ethanol solution exhibits two intense absorption bands at  $3.2$  and  $5.9$  eV and one band with a lower intensity located at  $\sim 4.8$  eV.<sup>114</sup> As for thioindigo, the lowest-lying state is of  $\pi \rightarrow \pi^*$  type and mainly results from the HOMO  $\rightarrow$  LUMO excitation. The third state calculated at  $4.50$  eV with small intensity ( $f = 0.085$ ) is due to the two nearly degenerate configurations HOMO-1 $\rightarrow$ LUMO and HOMO  $\rightarrow$  LUMO + 1 and assigned to the band located in the experimental spectrum at  $4.8$  eV. The third band in the spectrum of coumarin 102 is relatively broad with a maximum  $\sim 5.9$  eV. According to the TDDFT calculations, this band is composed mainly of two transitions to the 10A and 11A states calculated at  $5.85$  and  $6.02$  eV, respectively. In this case, we observe some overestimation of the calculated intensities that may be caused by solvent effects. Note, however, that TDDFT errors of  $\sim 50\%$  for oscillator strengths, especially for higher-lying transitions, are not unusual and that the neglected vibronic effects (FC factors much smaller than unity) may also contribute to this error.

### *Transition Metal Complexes*

Describing the electronic structure of transition metal compounds remains a challenging goal in quantum chemistry in general. The importance of static correlation effects arising from near degeneracy within the metal  $d$ -shells causes difficulties in ab initio single-reference treatments (in TDDFT there is some implicit account of static EC). Additionally, the low quality of the Hartree-Fock orbitals for transition metal compounds complicates the application of approaches lacking appropriate orbital relaxation effects. The TDDFT method is currently the only one that can be applied routinely to these systems, especially when large compounds without any symmetry

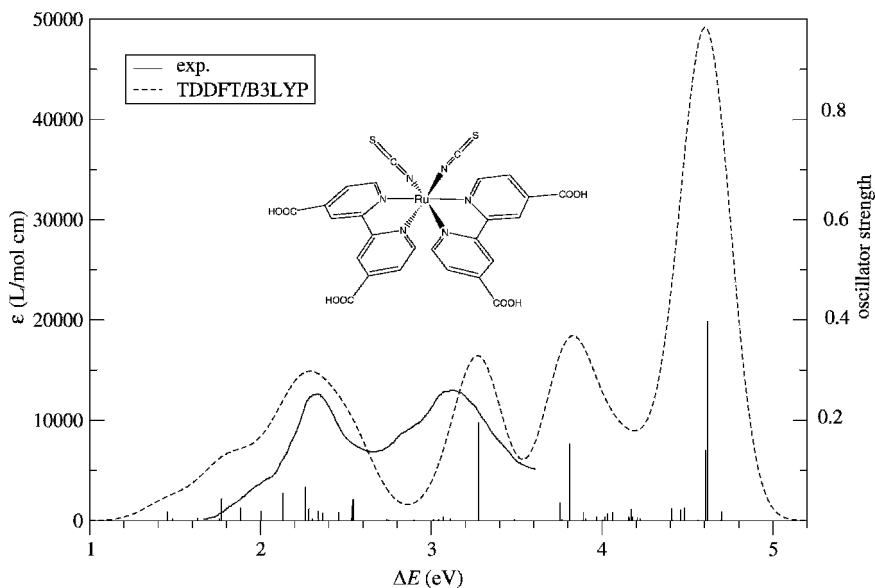


**Figure 15** Comparison of experimental and computed [B3LYP/SV(d)] UV spectra of the bipyridine–ruthenium complex. The theoretical  $\Delta E$  values are blue-shifted by 0.5 eV.

are considered (for CASPT2 investigations of the spectra of small TM compounds, see Ref. 11). Although in some cases semiempirical methods like INDO seem to be applicable<sup>119</sup> the DFT methods are more robust and even with nontrivial basis sets the calculation times are small enough to allow routine applications on “real” systems. For other applications of the TDDFT method to TM systems, see, for example, Ref. 120 and for a recent photochemical TDDFT study, see Ref. 121.

As an example, we present in this section a TDDFT study of the optical absorption spectrum of  $[\text{Ru}(4,4'\text{-COOH-}2,2'\text{-bpy})_2(\text{NCS})_2]$  (bpy = 2,2'-bipyridine) (see inset in Figure 15), a widely used charge-transfer sensitizer in nanocrystalline  $\text{TiO}_2$  solar cells. In the calculations, we considered the neutral system where the four carboxylic groups are protonated to represent a realistic model of the complex under the experimental conditions<sup>122</sup> (water solutions at  $\text{pH} < 1.5$ ). The geometry optimization of the complex results in a pseudo-octahedral structure with  $C_2$  symmetry and a cis arrangement of the thiocyanate ligands. This optimization was carried out with the DFT-BP86<sup>108,109</sup> method employing SV(d) basis sets,<sup>123</sup> a quasirelativistic effective core potential (ECP) with 28 core electrons<sup>124</sup> and a  $[5s5p3d]$  AO basis set<sup>123</sup> for ruthenium. The excited-state calculations were carried out using the B3LYP functional. The calculated and the experimental absorption spectra are compared in Figure 15.

The experimental spectrum exhibits two bands in the visible and near-UV region centered at 2.3 and 3.1 eV,<sup>125</sup> respectively. The overall band shapes and their relative and absolute intensities are well described by the TDDFT approach and even the shoulder at  $\sim 1.9$  eV is predicted correctly. The underestimation of the calculated excitation energies by  $\sim 0.5$  eV may on the one hand be attributed to inabilities of the chosen density functional but on the other hand certainly includes solvation effects that have been studied in Ref. 126 in the framework of continuum models. The neglected effects of spin-orbit coupling may be on the order of 0.1–0.2 eV, which seems to be significantly smaller than the differences obtained with various density functionals. As can be seen by the vertical lines included in Figure 15, which indicate the position and  $f$  values of the individual transitions, the density of electronic transitions even in the low-energy range is quite high. For the first two bands,  $\sim 25$  electronic states have to be considered, which increases to  $\sim 60$  in the range up to 5 eV. The TDDFT method is the only one that is currently applicable in such situations.

The character of the electronic transitions is usually analyzed in terms of the contributing single excitations. Although this is sometimes problematic due to extensive orbital and configuration mixing, the analysis is straightforward in our particular example. The first absorption band has strong multi-configurational character and involves excitations from the highest occupied to the lowest unoccupied  $\pi^*$  molecular orbitals. The many orbitals close to the HOMO are mainly of ruthenium  $d$ -orbital character with significant amplitudes on the isothiocyanate ligands. The second and the third absorption band involve excitations from a second set of metal  $d$  orbitals, to the lowest unoccupied  $\pi^*$  molecular orbitals, which can be characterized as metal–ligand charge-transfer (MLCT) bands. The fourth band at  $\sim 4.6$  eV is very intense and can easily be assigned to intraligand ( $\pi \rightarrow \pi^*$ ) excitations.

### *Open-Shell Systems: The Phenoxy Radical*

Due to its crucial role in combustion chemistry and biology, the phenoxy radical has been the subject of intense experimental and theoretical studies for many years (for recent work, see Ref. 127 and references cited therein). For these reasons we present it here as an example of UV spectroscopy of (neutral) radicals (for the application of DFT to the spectra of aromatic radical cations, see, e.g., Ref. 128 and for results of MRCI computations, see Ref. 129). The phenoxy radical is well known as a difficult case for electronic structure methods because it requires a sophisticated treatment of electron correlation similar to closed-shell aromatic hydrocarbons.

In agreement with previous DFT studies,<sup>127</sup> we found a  ${}^2B_1$  ground state (assuming  $C_{2v}$  symmetry with  $yz$  being the molecular plane) corresponding to a singly occupied orbital (SOMO) of  $\pi$  type. The lowest excited state corresponds to a  $n \rightarrow \pi$ (D-S) transition of  $B_2$  symmetry, which is dipole-forbidden. A weak band observed experimentally at  $\sim 1.1$  eV (1120 nm) supports this

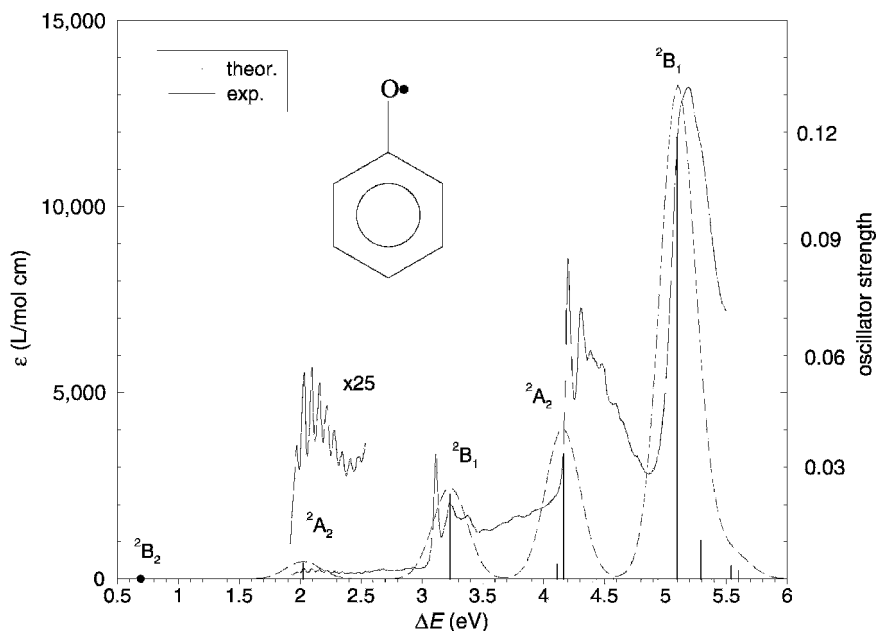


**Figure 16** Comparison of the computed [UTDDFT-B3LYP/TZV(d,p)] and experimental<sup>127</sup> UV spectra of the phenoxyl radical. The theoretical  $\Delta E$  values are shifted by  $-0.35$  eV.

prediction. The calculated vertical excitation energy of 1.04 eV is in almost perfect agreement with the experimental value. For the  $\pi\pi^*$  states of  $A_2$  and  $B_1$  symmetry the TDDFT-B3LYP/TZV(d,p) calculation yields energies slightly too high and thus a uniform red-shift of 0.35 eV has been applied in the simulation shown in Figure 16.

As can be seen from the comparison of the theoretical and experimental spectra, the unrestricted (U)TDDFT method provides a uniformly good description of the allowed transitions and the absolute and relative intensities are predicted quite accurately. The overestimation of all excitation energies seems to be due at least partially to the unrestricted treatment as indicated by a study using a recently developed restricted open-shell TDDFT<sup>22</sup> approach. Except for the  $1^2A_2$  state discussed below, the 0–0 transitions are most intense indicating only slight geometry changes compared to the ground state.

Figure 17 shows the vibrationally resolved spectrum obtained for the transition to the second lowest excited  $1^2A_2$  state. The theoretical treatment has been performed in the Franck–Condon approximation. The results are generally in very good agreement with the experimental data. The prominent progression with a spacing of  $\sim 500$   $\text{cm}^{-1}$  results from a totally symmetric (in-plane) CC stretching–bending mode. The relatively high intensities of the

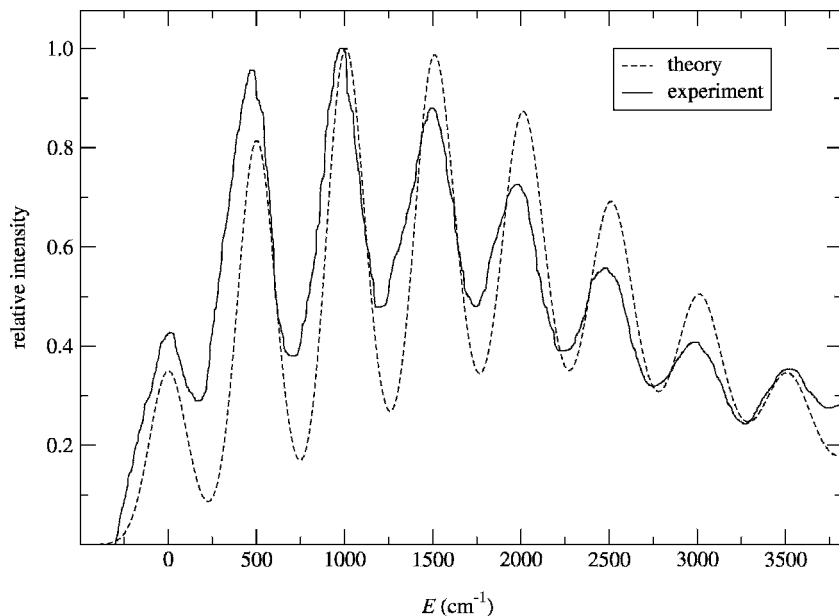


**Figure 17** Comparison of the computed [UTDDFT-B3LYP/TZV(d,p)] and experimental<sup>127</sup> UV band of the  $1^2A_2$  state of the phenoxyl radical. The 0–0 transition energy is set to zero.

0–1, 0–2, and 0–3 vibrational transitions can be explained by the geometries of the phenoxyl radical in the ground and excited states and the nature of the normal modes. The  $X^2B_1$  ground state has a partially chinoid structure with short C–O (1.25 Å) and C2–C3/C5–C6 (1.37 Å) bond lengths. The C–C bonds elongate in the  $1^2A_2$  state to  $\sim 1.43$  Å, thus matching almost exactly the geometric changes induced by the above mentioned stretching–bending mode. This example clearly shows how a vibrational analysis can reveal structural details of the corresponding states. Further examples of this type will be discussed in a later section.

#### *Open-Shell Systems: Excited-State Absorption of Naphthalene*

Excited-state absorption (ESA) is a type of electronic spectroscopy for which only a few theoretical studies have been performed (for a recent study on the singlet–singlet ESA spectrum of azulene, see Ref. 130 and for some benchmark calculations on small molecules, see Ref. 131). From the experimental point of view ESA is a very important topic in photophysical (kinetic) investigations of energy, electron or hydrogen-transfer processes. Although in principle all excited states of a molecule show a distinct electronic absorption spectrum, only the ESA spectra of the lowest excited state in each multiplicity (i.e.,  $S_1$  or  $T_1$ ) are usually accessible experimentally. Because of the short

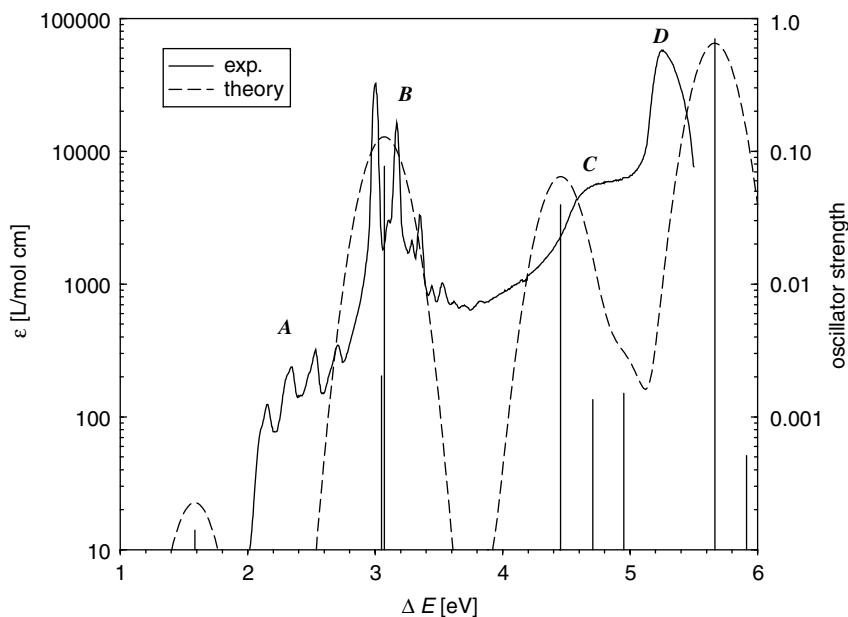


**Figure 18** Comparison of the computed (UTDDFT-B3LYP/cc-pVDZ) and experimental<sup>132</sup> triplet-triplet absorption spectra of naphthalene. Note the logarithmic intensity scale.

lifetime (low concentration) of excited molecules, special experimental (laser)-techniques are employed in ESA spectroscopy. Furthermore, background absorption by molecules in the ground state or by photoproducts need to be accounted for by taking difference spectra. Similar to the case of radicals, ESA spectra usually start in the visible and, sometimes, bands are observed even in the IR region ( $>1000$  nm).

The naphthalene molecule, which is used as an example here, has a lowest triplet state of  $B_{2u}$  symmetry and  $\pi \rightarrow \pi^*$  ( $L_a$ ) character. The dipole allowed transitions that are polarized in the plane of the molecule thus belong to transitions to  $A_g$  and  $B_{1g}$  excited states. The results of the unrestricted TDDFT-B3LYP treatment are shown in comparison with the experimental spectrum in Figure 18.

The assignments of the most intense bands seen in the experimental spectrum (bands B-D) agree with those from previous semiempirical PPP-type calculations<sup>132</sup> and will not be discussed here. Substantial disagreement between the theoretical and experimental data is observed only for the band A assigned to the  $1^3A_g$  state that is calculated too high by  $\sim 0.5$  eV. The transition to the  $1^3B_{1g}$  state (band B) is described almost perfectly while the

predicted excitation energies for band C and D show the typical TDDFT errors on the order of  $\pm 0.2$ – $0.4$  eV. Note, however, that the relative description for the different states is worse compared to the phenoxyl radical where a global shift of all excitation energies yields a satisfactory agreement with experiment. This is because of the more complicated electronic structure of the naphthalene  $T_1$  state (two vs. one open shell for the phenoxyl radical), which seems not to be described well enough by the simple TDDFT treatment. Furthermore, due to technical limitations it is currently not possible to check the degree of spin-contamination of the excited states ( $\langle \hat{S}^2 \rangle$  expectation value). Conclusive answers about the applicability of TDDFT in this area of spectroscopy requires more detailed work on other systems.

## Circular Dichroism

### *2,3-(S,S)-Dithiadecalin*

The nature of the chromophore of a molecule has a major influence on the corresponding CD spectroscopic properties. If the chromophore itself is chiral, it is denoted as being “inherently chiral”, whereas the term “inherently achiral” is used for locally achiral chromophores that are disturbed by their chiral surrounding (for a more detailed classification, see Ref. 133). The strength of the Cotton effect (rotatory strengths) provided by molecules containing an inherently chiral chromophore usually exceeds what is found for a molecule containing an inherently achiral chromophore by an order of magnitude.

The dithiadecalin (DTD) molecule (see inset in Figure 19) is characterized by the local chiral disulfide chromophore. Its first two transitions are expected to be of valence character and can be understood as single excitations out of the lone-pair orbitals at the sulfur atoms into the corresponding  $\sigma(SS)^*$  orbital. However, the  $\Delta \langle r^2 \rangle$  values of the transitions indicate significantly more diffuse character than expected for pure valence excited states.

To account for this fact, the TDDFT-B3LYP calculations of the spectra have been carried out with a TZV(2df) basis set augmented with diffuse functions at the sulfur atoms as well as at the neighboring carbon atoms and a TZV(d,p) basis set for the remaining atoms. The B3LYP/TZV(d,p) ground-state geometry has been used for these calculations. The theoretical spectrum has been blue shifted by 0.39 eV to match the experimental band A.

The experimental spectra of DTD<sup>134</sup> have been recorded in hexane. Keeping in mind the above described diffuse character of all excited states in DTD, an unbalanced theoretical description of states with stronger Rydberg character is to be expected when gas-phase data are compared with those from the condensed phase (Pauli-repulsion between the Rydberg state and solvent molecule wave functions). Figure 19, however, shows an almost perfect match between the theoretical gas-phase and experimental CD spectrum in the entire energy range. Even band C, which is theoretically predicted to have almost

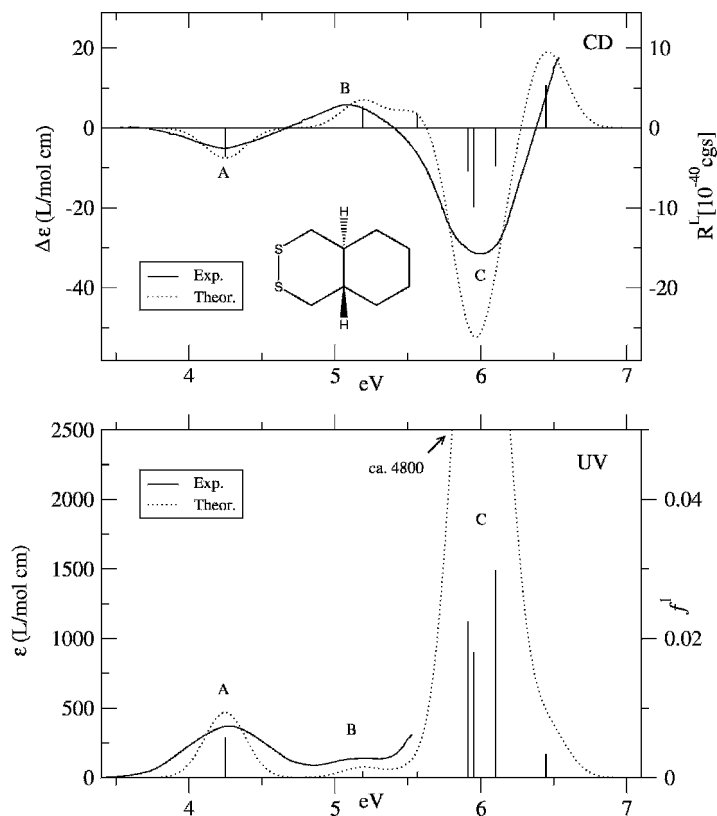


**Figure 19** Comparison of the experimental and computed [TDDFT-B3LYP/aug-TZV(2df)] UV and CD spectra for 2,3-(*S,S*)-dithiadecalin. The theoretical spectra have been blue-shifted by 0.39 eV.

exclusively Rydberg contributions, is described very well. It is pointed out here that the prevailing opinion that the excitation energies of Rydberg states are generally blue-shifted when going from the gas to the condensed phase<sup>6</sup> has been questioned recently for some molecules.<sup>135</sup> It should also be mentioned here that theoretical methods to describe the solvent effects on excited electronic states beyond simple electrostatics (i.e., continuum models) are in fact not yet developed.

The comparison with the UV spectrum shows an important advantage of CD over conventional UV spectroscopy for chiral molecules. Because the CD is a signed quantity, the band B is considerably better separated in the CD spectrum. If the bands would lie even closer to each other such that they could no longer be resolved by UV spectroscopy, CD spectroscopy would still yield two well-separated bands since the corresponding Cotton effects are oppositely signed.

*(M)*-[6]Helicene

Hexahelicene is one of the most widely studied molecules in theoretical CD spectroscopy (see, e.g., Refs. 47 and 136 and references cited therein). The system is rather large [120 valence electrons, 590 basis functions with a TZV(d,p) AO basis] and  $\sim 15$ – $20$  excited states are necessary to describe the experimental spectrum entirely. This example is presented here to show that correlated ab initio treatments are also applicable for such cases. The simplified coupled-cluster model CC2 together with the RI approximation is used and compared to the standard TDDFT-B3LYP approach.

The experimental CD spectrum (see Figure 20) consists of two very intense CD bands with opposite sign at 5.1 eV (240 nm, F) and 3.8 eV (320 nm, C). Shoulders (B, D, and E), and a very weak band (A) can, however, be clearly identified. With the exception of the region of band D, which is predicted with the wrong CD sign in both calculations, the theoretical data are in good agreement with the experimental spectrum; that is to say, all bands have a clear correspondence to calculated states. The theoretical excitation energies from CC2 have been red-shifted by 0.22 eV, which is on the order

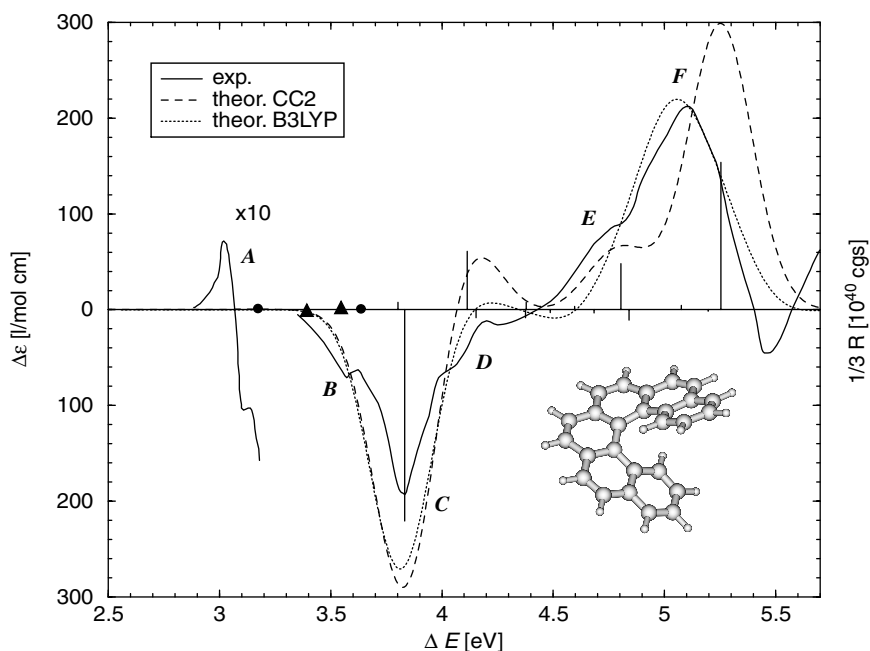


**Figure 20** Comparison of the experimental and computed [TZV(d,p) AO basis, B3LYP optimized geometry] CD spectra for *(M)*-[6]helicene. The theoretical spectra have been shifted by 0.20 (B3LYP) and  $-0.22$  eV (CC2), respectively. The filled circles/triangles indicate the two lowest states with small intensity obtained by CC2/TDDFT-B3LYP. The vertical lines correspond to results from the CC2 method.

of the expected solvent effect. Further enlarging of the AO basis would bring the CC2 data in even closer agreement with experiment (estimated effect of  $\sim 0.1\text{--}0.2$  eV). The TDDFT-B3LYP error is of opposite sign where the excitation energies are underestimated by  $\sim 0.2$  eV. The CC2 results are furthermore superior to those from TDDFT with respect to the splitting between the lowest  $L_b$  (band A) and  $L_a$  (band B) states. The larger error for the high-energy band F may be explained by some deficiencies of the TZV(d,p) AO basis set used, which lacks diffuse components as well as requisite higher angular momentum functions that are more important for explicitly correlated treatments than in DFT.

The computed intensities are also in reasonable agreement with experiment. The small  $R$  value for the  $L_b$  transition [ $-0.8 \times 10^{-40}$  cgs (CC2) vs.  $-1.6 \times 10^{-40}$  cgs (exp.)<sup>137</sup>] is predicted correctly with CC2 but has the wrong sign with TDDFT. However, this and the following  $L_a$  transition (band B) gain intensity by vibronic coupling with the close-lying intense  $B_b$  state and thus, results from vertical treatments should be taken cautiously.

When judging the accuracy of CC2 with respect to the TDDFT method, one should also consider the necessary computation times. While the TDDFT calculation was completed in  $\sim 15$  hours (on a PIII/1.4-GHz machine), the CC2 treatment took  $> 11$  days, which corresponds to a timing ratio of  $\sim 18$ . As mentioned before, the best strategy is thus to first calibrate the chosen density functional(s) by comparison with ab initio approaches on smaller (but structurally similar) molecules (in our example, e.g., [3]- or [4]helicene) and finally to perform the calculation on the large target system using only the cheaper TDDFT method.

### *(2S)-Tricarbonyl- $\eta^4$ -pentadi-2,4-enal-iron*

As mentioned in a previous section, the description of the electronic spectra of transition metal compounds in low-oxidation states is relatively complicated. When applying DFT-based methods, it is recommended that one carefully investigate the influence of the selected density functional. This is of particular importance here because there are currently no ab initio methods on which the TDDFT approaches can be calibrated. As an example we present a study of the CD spectrum of (2S)-tricarbonyl- $\eta^4$ -pentadi-2,4-enal-iron (ITP, for details, see Ref. 49). The molecule contains two achiral chromophores [pent-2,4-dienal and the  $\text{Fe}(\text{CO})_3$  fragment] which, attached to each other, form the chiral system. The spectroscopic activity of ITP in the near-UV originates mainly from  $3d(\text{metal}) \rightarrow \pi^*$  excitations. As a result of the similar energies of several electronic configurations, extensive mixing is observed including various  $n \rightarrow \pi^*$  states. Hence, it is understandable that the electronic nature of the excited states in ITP is described very differently depending on which method is applied. Furthermore, the energetic ordering and character of the MOs differs substantially between Hartree-Fock based and DFT approaches as well as between different DFT functionals. A reasonable direct comparison of the

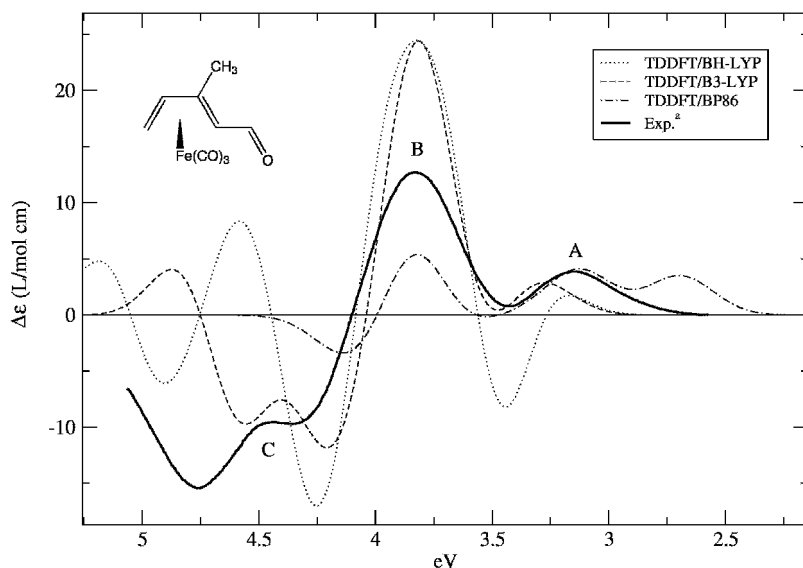


**Figure 21** Comparison of the experimental and computed CD spectra for the (2*S*)-tricarbonyl- $\eta^4$ -pentadi-2,4-enal-iron complex. The theoretical excitation energies have been shifted by  $-0.31$  (BHLYP),  $0.02$  (B3LYP), and  $0.21$  eV (BP), respectively (positive values refer to a blue-shift). The simulations include the contributions from the 15 lowest excited states.

results with the help of an MO based classification of the excited states is therefore not possible so, only the simulated spectra without any transition assignment are presented here. Figure 21 shows a comparison of experimental and theoretical data [SV(*d*) basis set for C, H, O and a [5*s*3*p*2*d*] set for Fe].

Inspection of Figure 21 shows relatively good agreement of the TDDFT-B3LYP spectrum with its experimental counterpart. The simulation with the BHLYP functional yields wrong signs for parts of bands A and C while the BP data seem to have little “overlap” with experiment. Strong dependencies of the results on the chosen density functional are not uncommon for more complicated systems. This type of dependency is the most severe drawback of the TDDFT method. In the original publication concerning this planar-chiral system,<sup>49</sup> conformational effects (cis vs. trans orientation of the carbonyl group) were investigated. The conformational preference seems to be resolvable by comparison of experiment with theory.

## Vibrational Structure

The shape and width of an absorption band in the visible region of the spectrum determines our color impression and is thus of fundamental importance in the area of dye chemistry. Theoretical simulations of the vibronic structure

of absorption bands allow us to evaluate the accuracy of the methods for finding the minimum energy geometries and vibrational frequencies. Systematic studies of the vibrational structures of the absorption bands for large molecules have not been performed to date. A few investigations have been undertaken using semiempirical<sup>138</sup> or CIS<sup>139</sup> methods that however, did not give fully satisfactory results. For the first time, we will show here that reliable predictions can be obtained in the framework of TDDFT. This has become possible due to the recently developed analytical TDDFT excited-state gradient.<sup>140</sup> In fact, it will be shown that the excited-state geometries and vibrational frequencies from (TD)DFT are much more accurate than the corresponding excitation energies (see also Ref. 141).

### Anthracene

As a first example, let us consider the vibronic structure of the first absorption band in the UV spectrum of anthracene. In agreement with experiment, the TDDFT calculation gives an  $S_1$  state with  $B_{2u}$  symmetry and a vertical excitation energy of 3.23 eV [ $\Delta E^{0-0}(\text{exp.}) = 3.43$  eV]. This band can be described by a HOMO  $\rightarrow$  LUMO excitation and in the Platt nomenclature (perimeter model) it is denoted as the  $L_a$  state. Both states were optimized at the (TD)DFT-B3LYP/TZV(d,p) level in  $D_{2h}$  symmetry.

A comparison of the spectrum simulation with a low-resolution gas-phase absorption spectrum<sup>26</sup> is shown in Figure 22. This type of spectrum is

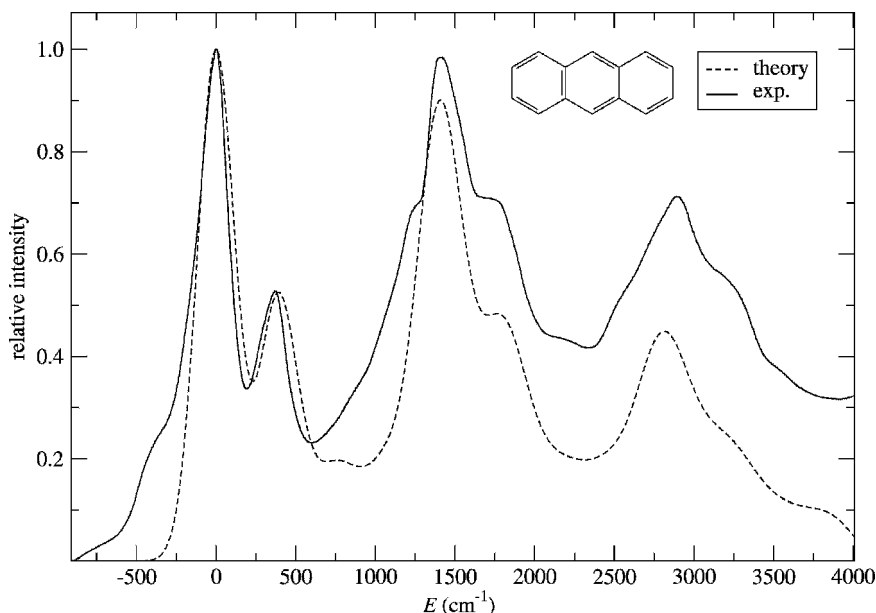


Figure 22 Comparison of the computed [TDDFT-B3LYP/TZV(d,p)] and experimental<sup>26</sup> UV spectra for the  $^1L_a$  state of anthracene. The 0-0 transition energy is set to zero.

typical for large systems (normal UV spectra), and has therefore been chosen for discussion here. The theoretical intensities were obtained within the FC approximation at 0 K and the individual transitions were broadened by Gaussian shape functions using a half-width of  $\sigma = 165 \text{ cm}^{-1}$ .

The computed spectrum shows a good agreement with its experimental counterpart over the entire energy range. This indicates that the geometry and frequency-normal mode changes between the two states are much better described by DFT than are the excitation energies (the DFT error for  $\Delta E^{0-0}$  is  $-0.59 \text{ eV}$ ). The weak shoulders (hot-bands) located  $\sim 300\text{--}750 \text{ cm}^{-1}$  below the 0-0 transition cannot be described by the present calculation. Although the description of hot-bands is straightforward in principle (by thermal population of vibrational ground-state levels), the current implementation of the recursive integral algorithm leads to unacceptably long computation times in such cases. As expected, the FC approximation seems to be very good for a dipole-allowed transition as considered here. The gradual increase of the experimental intensity relative to the calculated one in Figure 22 may arise from a nonhorizontal baseline in the measured spectrum. Furthermore, the second, less intense transition to the  $S_2$  state ( $L_b$ ) hidden under the  $L_a$  band may also contribute to this intensity mismatch. All vibronic transitions with a high intensity correspond to excitations of totally symmetric normal modes with a maximum excitation of two quanta in a single vibration.

### *Octatetracene*

Polyenes represent a class of widely studied molecules. Their ability to undergo photochemical isomerizations is exploited by Nature to transduce radiative energy into chemical energy and thus, these systems perform vital functions in many biochemical processes. *All-trans* octatetraene is used here as a model system to assess the ability of DFT methods to predict the important spectroscopy of this and related systems.

A weak first absorption is found experimentally ( $\Delta E^{0-0} = 3.59 \text{ eV}$ ) corresponding to the electric dipole-forbidden  $1A_g \rightarrow 2A_g$  transition. The second (intense) band results from the allowed  $1A_g \rightarrow 1B_u$  transition ( $\Delta E^{0-0} = 4.41 \text{ eV}$ ). This situation is challenging for any theoretical method because the character of both states is very different (single-configurational, ionic  $1B_u$  state vs. multiconfigurational, covalent  $2A_g$  state with significant contributions from double excitations).

All calculations were performed at the (TD)DFT-B3LYP/TZV(d,p) level employing  $C_{2b}$  symmetry. In contrast to the experimental data, the TDDFT calculation yields an  $S_1$  state with  $B_u$  symmetry ( $\Delta E^{\text{el}} = 4.05 \text{ eV}$ ) and the  $2A_g$  state as the second one ( $\Delta E^{\text{el}} = 4.89 \text{ eV}$ ). This error can be traced to the systematic underestimation of excitation energies for ionic states with TDDFT-B3LYP.<sup>35</sup> Because of the adiabatic approximation used in the TDDFT treatments, the  $2A_g$  state is described solely by a mixing of  $\text{HOMO} \rightarrow \text{LUMO} + 1$  and  $\text{HOMO}-1 \rightarrow \text{LUMO}$  single excitations. It lacks

the important HOMO–LUMO double excitation that has  $\sim 30\%$  weight in MR-MP2 wave functions. Thus we show here how such deficiencies of the theoretical treatment transfer to the description of the geometries and vibrational frequencies, and finally to the simulated vibronic structure.

A comparison of computed (FC approximation, broadened by Lorentzian functions with a half-width of  $\sigma = 20 \text{ cm}^{-1}$ ) and experimental gas-phase spectra<sup>30</sup> for the  $1B_u$  state is shown in Figure 23. Compared to the previous example, the theoretical description using B3LYP is worse. An obvious deviation from experiment is the relatively strong progression of the nontotally symmetric normal mode with a frequency of  $143 \text{ cm}^{-1}$ . This indicates an overestimation of the frequency change for this mode upon electronic excitation. Because ionic  $\pi \rightarrow \pi^*$  states benefit from the inclusion of “exact” HF exchange,<sup>25</sup> the calculation was repeated with the BHLYP functional (EEX = 50%). As can be seen from Figure 23, this significantly improves the description of the vibronic structure that is now in acceptable agreement with experiment over the entire energy range. Test calculations using TDHF (EEX = 100%) yield results that deviate more strongly from experiment (not shown) indicating that there is some (state-dependent!) optimum of exchange mixing in the density functionals.

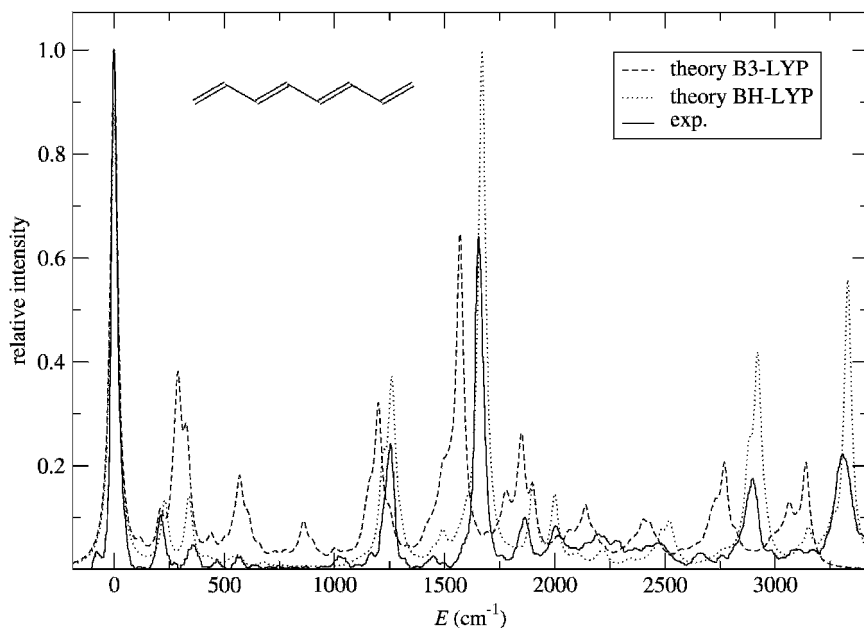


**Figure 23** Comparison of the computed [TDDFT/TZV(d,p)] and experimental<sup>30</sup> spectra for the  $1B_u$  state of octatetrene. The 0–0 transition energy is set to zero.

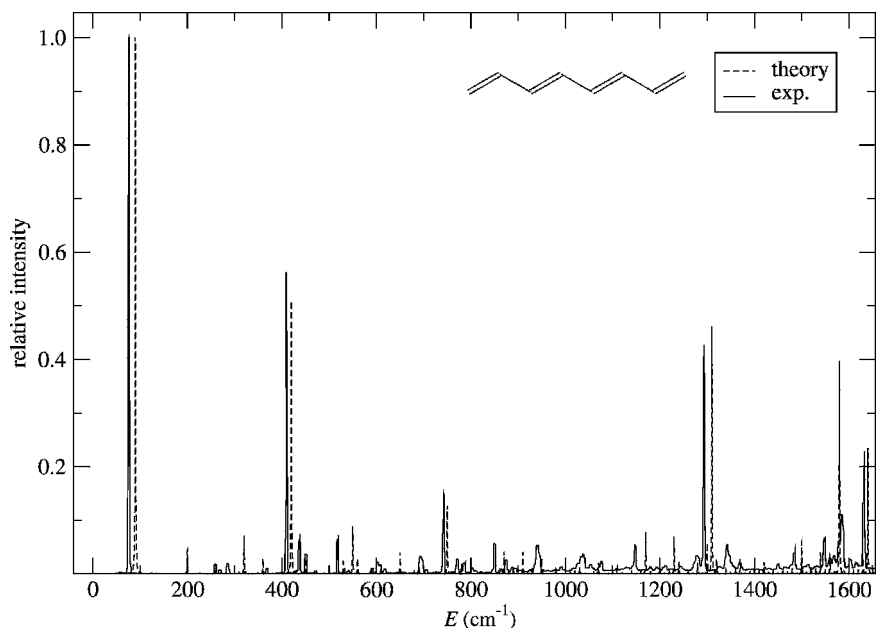


**Figure 24** Comparison of the computed [TDDFT-B3LYP/TZV(d,p)] and experimental<sup>31</sup> spectra for the  $2A_g$  state of octatetraene. The 0–0 transition energy is set to zero.

The dipole forbidden  $1A_g \rightarrow 2A_g$  transition must be treated at the Herzberg–Teller level (see earlier section) including the derivatives of the electronic transition dipole moment. These results are shown in Figure 24 in comparison with the experimental jet spectrum.<sup>31</sup> The computed intensities were broadened with Lorentzian functions using a half-width of  $\sigma = 0.5 \text{ cm}^{-1}$ .

Somewhat surprisingly, the calculated spectrum shows an almost perfect agreement with the experiment. This seems to indicate that either the density functional implicitly accounts for the missing double excitation (see also Ref. 142) or that its influence on the shape of the excited-state potential energy surface is small or similar to that of the HOMO  $\rightarrow$  LUMO + 1 and HOMO – 1  $\rightarrow$  LUMO excitations. Based upon the intensity inducing  $b_u$  mode with a frequency of  $94 \text{ cm}^{-1}$ , which leads to mixing of the  $S_1$  and  $S_2$  states, several excitations of totally symmetric modes with low quantum numbers are observable.

### *Formaldehyde*

The harmonic approximation is essential for computing the vibrational structure of electronic bands for large molecules. For more “floppy” (low-energy) nuclear motions (like torsions and bendings), it is inadequate. Here, we present an example of how the harmonic treatment of such motions affects the shape of the calculated spectra. The electric dipole forbidden  $n \rightarrow \pi^*$

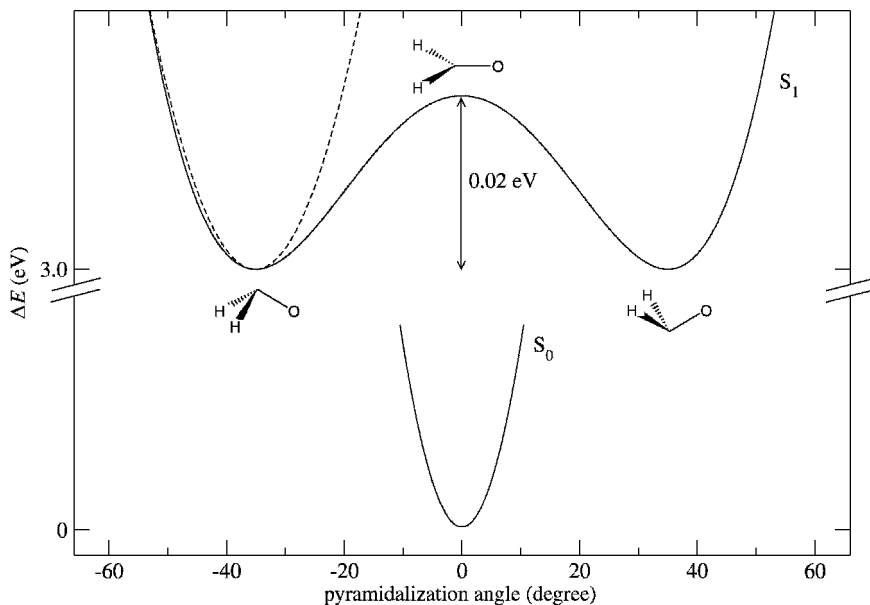


**Figure 25** Ground and first excited-state potential energy curves [TDDFT-B3LYP/TZV(d,p)] along the pyramidalization coordinate of formaldehyde. For comparison, the dashed line shows the harmonic potential.

transition of formaldehyde is used to illustrate this issue (for other TDDFT treatments of the excited-state surfaces of this molecule, see Ref. 143).

The geometry of the ground state was optimized at the DFT-B3LYP(TZV(d,p)) level in  $C_{2v}$  symmetry. The TDDFT calculation yields an  $S_1$  state with  $A_2$  symmetry and a vertical excitation energy of 3.99 eV ( $\Delta E^{0-0} = 3.56$  eV, exp. 3.51 eV<sup>144</sup>), which can be described by the HOMO (lone-pair)  $\rightarrow$  LUMO ( $\pi^*$ ) single excitation. The geometry optimization of the  $S_1$  state was carried out in  $C_s$  symmetry. In agreement with experimental data, we obtain a nonplanar minimum for the excited state with a pyramidalization angle of 34.9° (experimentally 33.6°<sup>145</sup>), which lies only 0.02 eV (experimentally 0.044 eV<sup>145</sup>) below a planar transition state for inversion (see Figure 25). Based on a Herzberg–Teller treatment, a simulation of the vibronic structure was performed and the obtained intensities were broadened with Lorentzian functions with a half-width of  $\sigma = 50$  cm<sup>-1</sup>.

A comparison of the calculated and experimental gas-phase spectra<sup>144</sup> (see Figure 26) clearly shows the limits of a harmonic treatment. Although the overall shape of the spectrum is reproduced quite well including the dominant C–O stretch progression, the inversion doubling of most peaks due to the double-minimum potential is obviously missing. Because such situations can

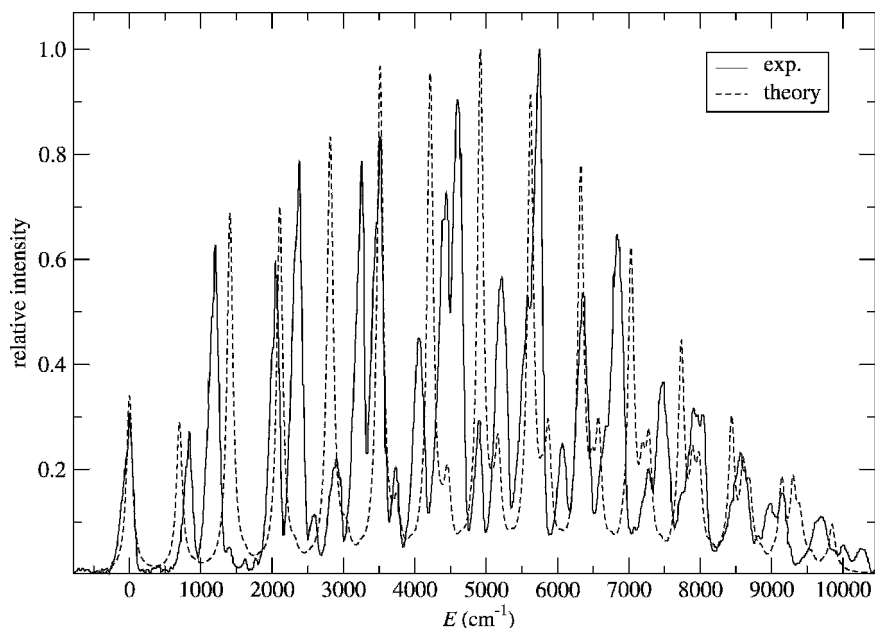


**Figure 26** Comparison of computed [TDDFT-B3LYP/TZV(d,p)] and experimental<sup>144</sup> absorption spectra of formaldehyde. The 0–0 transition energy is set to zero.

also be found in larger systems (although the consequences for the shape of the spectra are expected to be of lesser importance) these limits of the currently feasible theoretical treatments must be kept in mind.

---

## SUMMARY AND OUTLOOK

In this chapter, we have attempted to demonstrate that present-day quantum chemical electronic structure methods can provide an effective tool for predicting and interpreting electronic spectra of large molecules. This includes the calculation of vertical and 0–0 excitation energies, relative and absolute intensities, as well as details of vibrational features of absorption bands. A wide range of structurally different molecules and transitions between states of various characteristics have been successfully considered. This fact in turn strongly indicates that electronically excited states can be satisfactorily described by some of the above mentioned theoretical methods. The development of density functional based methods in particular has opened new areas of application that 10 years ago would have been “unthinkable”. Progress has also emerged in pure ab initio (wave function) approaches in

recent years. These systematically improvable methods are still necessary to calibrate and test the density functionals or even other more approximate techniques. Because of the complexity of most excited-state problems, combined approaches using very different theoretical methods from all areas of quantum chemistry are strongly recommended because a multifaceted approach will increase the overall reliability of the predictions. On the other hand, there is still a long way to go to improve existing theories and challenging problems remain to be solved. Beside the constant necessity to increase accuracy and applicability, the two issues of solvent effects on electronic spectra and the development of treatments for large and flexible systems are relevant topics for future researchers.

---

## ACKNOWLEDGMENTS

Dr. Christian Mück-Lichtenfeld is thanked for technical support. Many of the calculations have been performed by my students C. Diedrich, M. Dierksen, and M. Parac. The continuous support of the program system TURBOMOLE<sup>146</sup> (which has been used in all calculations) by R. Ahlrichs and the Quantum Chemistry Group at Karlsruhe, Germany, is also acknowledged. This work was supported by the Fonds der Chemischen Industrie, the Deutsche Forschungsgemeinschaft in the framework of the SFB 334 and 424 and by the BASF AG, Ludwigshafen.

---

## REFERENCES

1. T. Helgaker, P. Jørgensen, and J. Olsen, *Molecular Electronic-Structure Theory*, Wiley, New York, 2000.
2. S. D. Peyerimhoff, in *Encyclopedia of Computational Chemistry*, Wiley, New York, 1998, pp. 2646–2664. Spectroscopy: Computational Methods.
3. J. N. Murrel, *The Theory of the Electronic Spectra of Organic Molecules*, Methuen, London, 1963.
4. H. H. Jaffe and M. Orchin, *Theory and Applications of Ultraviolet Spectroscopy*, Wiley, New York, 1962.
5. N. Mataga and A. Kubota, *Molecular Interactions and Electronic Spectra*, Marcel Dekker, Inc., New York, 1970.
6. M. B. Robin, *Higher Excited States of Polyatomic Molecules*, Vol. 1–2, Academic Press, New York, 1975.
7. N. J. Turro, *Modern Molecular Photochemistry*, Benjamin Cummings, Menlo Park, CA, 1978.
8. J. Michl and V. Bonacic-Koutecky, *Electronic Aspects of Organic Photochemistry*, Wiley, New York, 1990.
9. M. Klessinger and J. Michl, *Excited States and Photochemistry of Organic Molecules*, VCH, New York, 1995.
10. B. O. Roos, M. Fülcher, P.-A. Malmqvist, M. Merchan, and L. Serrano-Andres, in *Quantum Mechanical Electronic Structure Calculations with Chemical Accuracy*, S. R. Langhoff, Ed., Kluwer Academic Publishers, Dordrecht, 1995, pp. 357–438. Theoretical Studies of Electronic Spectra of Organic Molecules.

11. B. O. Roos, K. Andersson, M. P. Fülcher, P.-K. Malmqvist, L. Serrano-Andres, K. Pierloot, and M. Merchan, *Adv. Chem. Phys.*, **18**, 219 (1996). Multiconfigurational Perturbation Theory: Applications in Electronic Spectroscopy.
12. M. Merchan, L. Serrano-Andres, M. P. Fülcher, and B. O. Roos, in *Recent Advances in Multireference Methods*, K. Hirao, Ed., World Scientific, Singapore, 1999, pp. 161–195. Multiconfigurational Perturbation Theory Applied to Excited States of Organic Compounds.
13. S. Tretiak and S. Mukamel, *Chem. Rev.*, **102**, 3171 (2002). Density Matrix Analysis and Simulation of Electronic Excitations in Conjugated and Aggregated Molecules.
14. C. Marian, in *Reviews in Computational Chemistry*, K. B. Lipkowitz and D. B. Boyd, Eds., Vol. 17, Wiley-VCH, New York, 2001, pp. 99–204. Spin–Orbit Coupling in Molecules.
15. B. A. Heß, C. M. Marian, and S. D. Peyerimhoff, in *Modern Electronic Structure Theory*, D. R. Yarkony, Ed., World Scientific, Singapore, 1995, pp. 152–278. Ab Initio Calculation of Spin–Orbit Effects in Molecules Including Electron Correlation.
16. C. Engemann, G. Köhring, A. Pantelouris, J. Hormes, S. Grimme, S. D. Peyerimhoff, J. Clade, F. Frick, and M. Jansen, *Chem. Phys.*, **221**, 189 (1997). Experimental and Theoretical Investigations of the X-Ray Absorption Near Edge Spectra (XANES) of  $P_4O_6$  and  $P_4O_6X$  ( $X = O, S, Se$ ).
17. M. Stener, G. Fronzoni, and M. de Simone, *Chem. Phys. Lett.*, **373**, 115 (2003). Time-Dependent Density Functional Theory of Core Electron Excitations.
18. P. Salek, O. Vahtras, J. Guo, Y. Luo, T. Helgaker, and H. Ågren, *Chem. Phys. Lett.*, **374**, 446 (2003). Calculations of Two-Photon Absorption Cross Sections by Means of Density-Functional Theory.
19. S. F. Mason, *J. Chem. Soc.*, 1263 (1959). The Electronic Spectra of N-Heteroaromatic Systems: Part 4. The Vibrational Structure of the  $n \rightarrow \pi^*$  Band of sym-Tetrazine.
20. A. D. Becke, *J. Chem. Phys.*, **98**, 5648 (1993). Density-Functional Thermochemistry. III. The Role of Exact Exchange.
21. P. J. Stevens, F. J. Devlin, C. F. Chabalowski, and M. J. Frisch, *J. Phys. Chem.*, **98**, 11623 (1994). Ab Initio Calculation of Vibrational Absorption and Circular Dichroism Spectra using Density Functional Force Fields.
22. Z. Rinkevicius, I. Tunell, P. Salek, O. Vahtras, and H. Ågren, *J. Chem. Phys.*, **119**, 34 (2003). Restricted Density Functional Theory of Linear Time-Dependent Properties in Open-Shell Molecules.
23. C. S. Page and M. Olivucci, *J. Comput. Chem.*, **24**, 298 (2003). Ground and Excited State CASPT2 Geometry Optimizations of Small Organic Molecules.
24. J. Fabian, L. A. Diaz, G. Seifert, and T. Niehaus, *J. Mol. Struct.*, **594**, 41 (2002). Calculation of Excitation Energies of Organic Chromophores: A Critical Evaluation.
25. M. Parac and S. Grimme, *J. Phys. Chem. A*, **106**, 6844 (2002). Comparison of Multireference Møller–Plesset Theory and Time-Dependent Methods for the Calculation of Vertical Excitation Energies of Molecules.
26. J. Ferguson, L. W. Reeves, and W. G. Schneider, *Can. J. Chem.*, **35**, 1117 (1957). Vapor Absorption Spectra and Oscillator Strengths of Naphthalene, Anthracene and Pyrene.
27. A. Amirav, U. Even, and J. Jortner, *J. Chem. Phys.*, **75**, 3770 (1981). Energetics and Intramolecular Dynamics of the Isolated Ultracold Tetracene Molecule in its First Singlet State.
28. M. Banasiewicz, I. Deperasińska, and B. Kozankiewicz, *J. Phys. Chem. A*, **107**, 662 (2003). Spectroscopic Characteristics of Pentacene in Shpol'skii Matrixes.
29. Y. Lou, J. Chang, J. Jörgensen, and D. M. Lemal, *J. Am. Chem. Soc.*, **124**, 15302 (2002). Octachloroazulene.
30. D. G. Leopold, V. Vaida, and M. F. Granville, *J. Chem. Phys.*, **81**, 4210 (1984). Direct Absorption Spectroscopy of Jet-Cooled Polyenes. I. The  $1^1B_u^+ \leftarrow 1^1A_g^-$  Transition of *trans,trans*-1,3,5,7-Octatetraene.

31. H. Petek, A. J. Bell, Y. S. Choi, K. Yoshihara, B. A. Tounge, and R. L. Christensen, *J. Chem. Phys.*, **98**, 3777 (1993). The  $2^1A_g$  State of trans,trans-1,3,5,7-octatetraene in Free Jet Expansions.
32. D. G. Leopold, R. J. Hemley, V. Vaida, and J. L. Roebber, *J. Chem. Phys.*, **75**, 4758 (1981). Direct Absorption Spectra of Higher Excited States of Jet-Cooled Monosubstituted Benzenes: Phenylacetylene, Styrene, Benzaldehyde and Acetophenone.
33. O. Dopfer, Ph.D. Dissertation, Technische Universität, München, 1994.
34. P. Imhof and K. Kleinermanns, *J. Phys. Chem. A*, **105**, 8922 (2001). Dispersed Fluorescence Spectra and Ab Initio Calculations of *o*-Cyanophenol.
35. S. Grimme and M. Parac, *Chem. Phys. Chem.*, **4**, 292 (2003). Substantial Errors from Time-Dependent Density Functional Theory for the Calculation of Excited States of Large  $\pi$ -Systems.
36. M. Parac and S. Grimme, *Chem. Phys.*, **292**, 11 (2003). A TDDFT Study of the Lowest Excitation Energies of Polycyclic Aromatic Hydrocarbons.
37. S. Tirapattur, M. Belletete, M. Leclerc, and G. Durocher, *J. Mol. Struct.*, **625**, 141 (2003). Study of Excited State Properties of Oligofluorenes by the Singles Configuration Interaction (CIS) Theoretical Approach.
38. H. Eyring, J. Walter, and G. E. Kimball, *Quantum Chemistry*, Wiley, New York, 1949.
39. P. W. Atkins and R. S. Friedman, *Molecular Quantum Mechanics*, Oxford University Press, Oxford, 1997.
40. T. H. Dunning, Jr., *J. Chem. Phys.*, **90**, 1007 (1989). Gaussian Basis Sets for Use in Correlated Molecular Calculations. I. The Atoms Boron Through Neon and Hydrogen.
41. R. A. Kendall, T. H. Dunning, Jr., and R. J. Harrison, *J. Chem. Phys.*, **96**, 6796 (1992). Electron Affinities of the First-Row Atoms Revisited. Systematic Basis Sets and Wave Functions.
42. C. W. Bauschlicher, Jr., and S. R. Langhoff, *Theor. Chim. Acta*, **79**, 93 (1991). Computation of Electronic Transition Moments: the Length versus the Velocity Representation.
43. K. Nakanishi, N. Berova, and R. Woody, Eds., *Circular Dichroism*, VCH, Weinheim, 1994.
44. E. Charney, *The Molecular Basis of Optical Activity*, Wiley, New York, 1979.
45. J. A. Schellman, *Chem. Rev.*, **75**, 323 (1975). Circular Dichroism and Optical Rotation.
46. G. H. Wagniere, *Linear and Nonlinear Optical Properties of Molecules*, VCH, Weinheim, 1993.
47. S. Grimme, A. Sobanski, J. Harren, and F. Vögtle, *Eur. J. Org. Chem.*, 1491 (1998). Structure-Chiroptic Relations of Planar Chiral and Helical Molecules.
48. D. A. Lightner and J. E. Gurst, *Organic Conformational Analysis and Stereochemistry from Circular Dichroism Spectroscopy*, Wiley-VCH, New York, 2000.
49. C. Diedrich and S. Grimme, *J. Phys. Chem. A*, **107**, 2524 (2003). Systematic Investigation of Modern Quantum Chemical Methods to Predict Electronic Circular Dichroism Spectra.
50. S. Coriani, P. Jørgensen, A. Rizzo, K. Ruud, and J. Olsen, *Chem. Phys. Lett.*, **300**, 61 (1999). Ab Initio Determinations of Magnetic Circular Dichroism.
51. I. Özkan and L. Goodman, *Chem. Rev.*, **79**, 275 (1979). Coupling of Electronic and Vibrational Motions in Molecules.
52. J. Franck, *Trans. Faraday Soc.*, **21**, 536 (1925). Elementary Processes of Photochemical Reactions.
53. E. U. Condon, *Phys. Rev.*, **28**, 1182 (1926). A Theory of Intensity Distribution in Band Systems.
54. E. U. Condon, *Phys. Rev.*, **32**, 858 (1928). Nuclear Motions Associated with Electron Transitions in Diatomic Molecules.
55. G. Herzberg and E. Teller, *Z. Phys. Chem. B*, **21**, 410 (1933). Schwingungsstruktur der Elektronenübergänge bei Mehratomigen Molekülen.

56. F. Duschinsky, *Acta Physicochem. URSS*, **7**, 551 (1937). Zur Deutung der Elektronenspektren Mehratomiger Moleküle.
57. G. M. Sando and K. G. Spears, *J. Phys. Chem.*, **105**, 5326 (2001). Ab Initio Calculation of the Duschinsky mixing of Vibration and Nonlinear Effects.
58. I. Özkan, *J. Mol. Spectrosc.*, **139**, 147 (1990). Franck–Condon Principle for Polyatomic Molecules: Axis-Switching Effects and Transformation of Normal Coordinates.
59. E. V. Doktorov, I. A. Malkin, and V. I. Man'ko, *J. Mol. Spectrosc.*, **64**, 302 (1977). Dynamical Symmetry of Vibronic Transitions in Polyatomic Molecules and the Franck–Condon Principle.
60. R. Berger, C. Fischer, and M. Klessinger, *J. Phys. Chem. A*, **102**, 7157 (1998). Calculation of the Vibronic Fine Structure in Electronic Spectra at Higher Temperatures. 1. Benzene and Pyrene.
61. J. Neugebauer, M. Reiher, C. Kind, and B. A. Heß, *J. Comput. Chem.*, **23**, 895 (2002). Quantum Chemical Calculation of Vibrational Spectra of Large Molecules—Raman and IR Spectra for Buckminsterfullerene.
62. C. Kind, M. Reiher, J. Neugebauer, and B. A. Heß. SNF Version 2.2.1, Universität, Erlangen, 2003.
63. C. D. Sherrill and H. F. Schaefer, III, *Adv. Quant. Chem.*, **34**, 143 (1999). The Configuration Interaction Method: Advances in Highly Correlated Approaches.
64. R. J. Rico and M. Head-Gordon, *Chem. Phys. Lett.*, **213**, 224 (1993). Single-Reference Theories of Molecular Excited States with Single and Double Substitutions.
65. M. Head-Gordon, R. J. Rico, M. Oumi, and T. J. Lee, *Chem. Phys. Lett.*, **219**, 21 (1994). A Doubles Correction to Electronic Excited States from Configuration Interaction in the Space of Single Substitutions.
66. S. Grimme and M. Waletzke, *J. Chem. Phys.*, **111**, 5645 (1999). A Combination of Kohn-Sham Density Functional Theory and Multi-Reference Configuration Interaction Methods.
67. A. B. J. Parusel and S. Grimme, *J. Porphyrins Phthalocyanines*, **5**, 225 (2001). DFT/MRCI Calculations on the Excited States of Porphyrin, Hydroporphyrins, Tetraporphyrins, and Metalloporphyrins.
68. J. Tatchen, M. Waletzke, C. M. Marian, and S. Grimme, *Chem. Phys.*, **264**, 245 (2001). The Photophysics of Pyranthione: A Theoretical Investigation Focusing on Spin-Forbidden Transitions.
69. M. Kleinschmidt, J. Tatchen, and C. M. Marian, *J. Comput. Chem.*, **23**, 824 (2002). Spin-Orbit Coupling of DFT/MRCI Wavefunctions: Method, Test Calculations, and Applications to Thiophene.
70. C. M. Marian, F. Schneider, M. Kleinschmidt, and J. Tatchen, *Eur. Phys. J. (D)*, **20**, 357 (2002). Electronic Excitation and Singlet–Triplet Coupling in Uracil Tautomers and Uracil–Water Complexes, a Quantum Chemical Investigation.
71. M. Kleinschmidt Tatchen, C. M. Marian, M. Parac, and S. Grimme, *Z. Phys. Chem.*, **217**, 205 (2003). Quantum Chemical Investigation of Spin-Forbidden Transitions in Dithiosuccinimide.
72. H. J. J. Van Dam, J. H. Van Lenthe, and P. J. A. Ruttink, *Int. J. Quant. Chem.*, **72**, 5498 (1999). Exact Size Consistency of Multireference Møller–Plesset Perturbation Theory.
73. S. Grimme, M. Parac, and M. Waletzke, *Chem. Phys. Lett.*, **334**, 99 (2001). On the Importance of Third and Fourth-Order Corrections in Multi-Reference Møller–Plesset Theory.
74. B. O. Roos and K. Andersson, in *Modern Electronic Structure Theory*, D. R. Yarkony, Ed., World Scientific, Singapore, 1995, pp. 55–109. *Multiconfigurational Second-Order Perturbation Theory*.
75. B. O. Roos, K. Andersson, and M. P. Fülcher, *Chem. Phys. Lett.*, **192**, 5 (1992). Towards an Accurate Molecular Orbital Theory for Excited States: The Benzene Molecule.
76. P. Celani and H.-J. Werner, *J. Chem. Phys.*, **112**, 5546 (2000). Multireference Perturbation Theory for Large Restricted and Selective Active Space Reference Wave Functions.

77. J. J. W. McDoull, K. Peasley, and M. A. Robb, *Chem. Phys. Lett.*, **148**, 183 (1988). A Simple MCSCF Perturbation Theory: Orthogonal Valence Bond Møller–Plesset 2 (OVBP2).
78. S. Grimme and M. Waletzke, *Phys. Chem. Chem. Phys.*, **2**, 2075 (2000). Multi-Reference Møller–Plesset Theory: Computational Strategies for Large Molecules.
79. L.-M. Frutos, O. Castano, and M. Merchán, *J. Phys. Chem. A*, **107**, 5472 (2003). Theoretical Determination of the Singlet–Singlet and Singlet–Triplet Electronic Spectra, Lowest Ionization Potentials, and Electron Affinity of Cyclooctatetraene.
80. R. G. Parr and W. Yang, *Density-Functional Theory of Atoms and Molecules*, Oxford University Press, Oxford, 1989.
81. W. Koch and M. C. Holthausen, *A Chemist’s Guide to Density Functional Theory*, Wiley-VCH, Weinheim, 2000.
82. E. K. U. Gross, J. F. Dobson, and M. Petersilka, *Top. Curr. Chem.*, **181**, 81 (1996). Density Functional Theory.
83. M. E. Casida, in *Recent Advances in Density Functional Methods*, Vol. 1, D. P. Chong, Ed., World Scientific, Singapore, 1995, pp. 155–213. Time-Dependent Density Functional Response Theory for Molecules.
84. H. Weiss, R. Ahlrichs, and M. Häser, *J. Chem. Phys.*, **99**, 1262 (1993). A Direct Algorithm for Self-Consistent Field Linear Response Theory and Application to C<sub>60</sub>: Excitation Energies, Oscillator Strengths and Frequency-Dependent Polarizabilities.
85. R. Bauernschmitt and R. Ahlrichs, *Chem. Phys. Lett.*, **256**, 454 (1996). Treatment of Electronic Excitations within the Adiabatic Approximation of Time Dependent Density Functional Theory.
86. S. Grimme, *Chem. Phys. Lett.*, **259**, 128 (1996). Density Functional Calculations with Configuration Interaction for the Excited States of Molecules.
87. S. Hirata and M. Head-Gordon, *Chem. Phys. Lett.*, **314**, 291 (1999). Time-Dependent Density Functional Theory within the Tamm–Dancoff Approximation.
88. H. Koch and P. Jørgensen, *J. Chem. Phys.*, **93**, 3333 (1990). Coupled Cluster Response Functions.
89. H. Koch, H. J. A. Jensen, P. Jørgensen, and T. Helgaker, *J. Chem. Phys.*, **93**, 3345 (1990). Excitation Energies from the Coupled Cluster Singles and Doubles Linear Response Function (CCSDLR). Applications to Be, CH<sup>+</sup>, CO, and H<sub>2</sub>O.
90. D. C. Comeau and R. J. Bartlett, *Chem. Phys. Lett.*, **207**, 414 (1993). The Equation-of-Motion Coupled-Cluster Method. Applications to Open- and Closed-Shell Reference States.
91. O. Christiansen, H. Koch, and P. Jørgensen, *Chem. Phys. Lett.*, **243**, 409 (1995). The Second-Order Approximate Coupled Cluster Singles and Doubles Model CC2.
92. C. Hättig and F. Weigend, *J. Chem. Phys.*, **113**, 5154 (2000). CC2 Excitation Energy Calculations on Large Molecules using the Resolution of the Identity Approximation.
93. A. Köhn and C. Hättig, *J. Chem. Phys.*, **119**, 5021 (2003). Analytical Gradients for Excited States in the Coupled-Cluster Model CC2 Employing the Resolution-of-the-Identity Approximation.
94. J. B. Foresman and E. Frisch, *Exploring Chemistry with Electronic Structure Methods*, Gaussian, Inc., Pittsburgh, 1996.
95. A. D. Becke, *J. Chem. Phys.*, **98**, 1372 (1993). A New Mixing of Hartree–Fock and Local Density Functional Theories.
96. D. J. Tozer and N. C. Handy, *J. Chem. Phys.*, **109**, 10180 (1998). Improving Virtual Kohn–Sham Orbitals and Eigenvalues: Application to Excitation Energies and Static Polarizabilities.
97. A. Dreuw, J. L. Weismann, and M. Head-Gordon, *J. Chem. Phys.*, **119**, 2943 (2003). Long-Range Charge-Transfer Excited States in Time-Dependent Density Functional Theory Require Non-local Exchange.

98. M.-S. Liao, Y. Lu, and S. Scheiner, *J. Comput. Chem.*, **24**, 623 (2003). Performance Assessment of Density-Functional Methods for Study of Charge-Transfer Complexes.
99. A. S. Zyubin and A. M. Mebel, *J. Comput. Chem.*, **24**, 692 (2003). Performance of Time-Dependent Density Functional and Green Functions Methods for Calculation of Excitation Energies in Radicals and for Rydberg Electronic States.
100. J. Spanget-Larsen, *Theor. Chem. Acc.*, **98**, 137 (1997). The Alternant Hydrocarbon Pairing Theorem and All-Valence Electrons Theory. An Approximate LCAO Theory for the Electronic Absorption and MCD Spectra of Conjugated Organic Compounds, Part 2.
101. W. Weber and W. Thiel, *Theor. Chem. Acc.*, **103**, 495 (2000). Orthogonalization Corrections for Semiempirical Methods.
102. F. Vögtle, A. Hüntten, E. Vodel, and S. Grimme, *Angew. Chem. Int. Ed. Engl.*, **40**, 2468 (2001). Novel Amide-Based Molecular Knots: Complete Enantiomeric Separation, Chiroptical Properties and Absolute Configuration.
103. M. Klessinger, T. Pötter, and C. van Wüllen, *Theoret. Chim. Acta*, **80**, 1 (1991). Semiempirical Valence-Electron Calculations of Excited State Geometries and Vibrational Frequencies.
104. A. Koslowski, M. E. Beck, and W. Thiel, *J. Comput. Chem.*, **24**, 714 (2003). Implementation of a General Multireference Configuration Interaction Procedure with Analytic Gradients in a Semiempirical Context using the Graphical Unitary Group Approach.
105. C. Sandorfy, Ed., *The Role of Rydberg States in Spectroscopy and Reactivity*, Kluwer Academic Publishers, Dordrecht, 1999.
106. A. S. Zyubin and A. M. Mebel, *J. Chem. Phys.*, **119**, 6581 (2003). Accurate Prediction of Excitation Energies to High-Lying Rydberg Electronic States: Rydberg States of Acetylene as a Case Study.
107. M. Merchán, B. O. Roos, R. McDiarmid, and X. Xing, *J. Chem. Phys.*, **104**, 1791 (1996). A Combined Theoretical and Experimental Determination of the Electronic Spectrum of Acetone.
108. A. D. Becke, *Phys. Rev. A*, **38**, 3098 (1988). Density-Functional Exchange-Energy Approximation with Correct Asymptotic Behaviour.
109. J. P. Perdew, *Phys. Rev. B*, **33**, 8822 (1986). Density-Functional Approximation for the Correlation-Energy of the Inhomogeneous Electron Gas.
110. F. D. Sala and A. Görling, *J. Chem. Phys.*, **116**, 5374 (2002). The Asymptotic Region of the Kohn-Sham Exchange Potential in Molecules.
111. F. D. Sala and A. Görling, *Int. J. Quant. Chem.*, **91**, 131 (2003). Excitation Energies of Molecules by Time-Dependent Density Functional Theory Based on Effective Exact Exchange Kohn-Sham Potentials.
112. P. Brint and L. O'Toole, *J. Chem. Soc. Faraday Trans.*, **87**, 2891 (1991). Multiphoton Ionisation Spectroscopy of the  $3s(2+2,1)$  and  $4s(3+1)$  Rydberg States of Acetone: Evidence for a Molecular Valence State at 153 nm.
113. R. M. Christie, *Colour Chemistry*, The Royal Society of Chemistry, Cambridge, UK, 2001.
114. U. Brackmann, *Lambdachrome Laser Dyes*, Lambda Physik AG, Göttingen, 2000.
115. A. Mühlpfordt, R. Schanz, N. Ernsting, V. Farztdinov, and S. Grimme, *Phys. Chem. Chem. Phys.*, **14**, 3209 (1999). Coumarin 153 in the Gas Phase: Optical Spectra and Quantum Chemical Calculations.
116. R. J. Cave and E. W. Castner, *J. Phys. Chem. A*, **106**, 12117 (2002). Time-Dependent Density Functional Theory Investigation of the Ground and Excited States of Coumarins 102, 152, 153, and 343.
117. R. J. Cave, K. Burke, and E. W. Castner, *J. Phys. Chem. A*, **106**, 9294 (2002). Theoretical Investigation of the Ground and Excited States of Coumarin 151 and Coumarin 120.
118. G. Haucke and R. Paetzold, *Photophysikalische Chemie Indigoider Farbstoffe*, Deutsche Akademie der Naturforscher Leopoldina, Halle (Saale), 1978.

119. M. C. Zerner, in *Reviews in Computational Chemistry*, K. B. Lipkowitz and D. B. Boyd, Eds., Vol. 2, Wiley-VCH, New York, 1991, pp. 313–365. Semiempirical Molecular Orbital Methods.
120. S. Zálaiš, I. R. Farrell, and A. Vlček, Jr., *J. Am. Chem. Soc.*, **125**, 4580 (2003). The Involvement of Metal-to-CO Charge Transfer and Ligand-Field Excited States in the Spectroscopy and Photochemistry of Mixed-Ligand Metal Carbonyls. A Theoretical and Spectroscopic Study of  $[\text{W}(\text{CO})_4(1,2\text{-ethylenediamine})]$  and  $[\text{W}(\text{CO})_4(\text{N,N-bis-alkyl-1,4-diazabutadiene})]$ .
121. T. P. M. Goumans, A. W. Ehlers, M. C. van Hemert, A. Rosa, E.-J. Baerends, and K. Lammertsma, *J. Am. Chem. Soc.*, **125**, 3558 (2003). Photodissociation of the Phosphine-Substituted Transition Metal Carbonyl Complexes  $\text{Cr}(\text{CO})_5\text{L}$  and  $\text{Fe}(\text{CO})_4\text{L}$ : A Theoretical Study.
122. M. K. Nazeeruddin, S. M. Zakeeruddin, R. Humphry-Baker, M. Jirousek, P. Liska, N. Vlachopoulos, V. Shklover, C.-H. Fisher, and M. Grätzel, *Inorg. Chem.*, **38**, 6298 (1999). Acid-Base Equilibria of (2,2'-Bipyridyl-4,4'-dicarboxylic acid)ruthenium(II) Complexes and the Effect of Protonation on Charge-Transfer Sensitization of Nanocrystalline Titania.
123. A. Schäfer, H. Horn, and R. Ahlrichs, *J. Chem. Phys.*, **97**, 2571 (1992). Fully Optimized Contracted Gaussian Basis Sets for Atoms Li to Kr.
124. D. Andrae, U. Häussermann, M. Dolg, H. Stoll, and H. Preuss, *Theor. Chim. Acta*, **77**, 123 (1990). Energy-Adjusted Ab Initio Pseudopotentials for the Second and Third Row Transition Elements.
125. J. E. Monat, J. H. Rodriguez, and J. K. McCusker, *J. Phys. Chem. A*, **106**, 7399 (2002). Ground- and Excited-State Electronic Structures of the Solar Cell Sensitizer bis(4,4'-dicarboxylato-2,2'-bipyridine)bis(isothiocyanato)ruthenium(II).
126. S. Fantacci, F. D. Angelis, and A. Selloni, *J. Am. Chem. Soc.*, **125**, 4381 (2003). Absorption Spectrum and Solvatochromism of the  $[\text{Ru}(4,4'\text{-COOH-2,2'-bpy})_2(\text{NCS})_2]$  Molecular Dye by Time Dependent Density Functional Theory.
127. J. G. Radziszewski, M. Gil, A. Gorski, J. Spanget-Larsen, J. Waluk, and B. J. Mroz, *J. Chem. Phys.*, **115**, 9733 (2001). Electronic States of the Phenoxy Radical.
128. S. Hirata, M. Head-Gordon, J. Szczepanski, and M. Vala, *J. Phys. Chem. A*, **107**, 4940 (2003). Time-Dependent Density Functional Study of the Electronic Excited States of Polycyclic Aromatic Hydrocarbon Radical Ions.
129. C. Niederal, S. Grimme, and S. D. Peyerimhoff, *Chem. Phys. Lett.*, **245**, 455 (1995). Ab Initio Theoretical Study of the Electronic Absorption Spectra of Polycyclic Aromatic Hydrocarbon Radical Cations of Naphthalene, Anthracene and Phenanthrene.
130. P. Foggi, F. V. R. Neuwahl, L. Moroni, and P. R. Salvi, *J. Phys. Chem. A*, **107**, 1689 (2003).  $S_1 \rightarrow S_n$  and  $S_2 \rightarrow S_n$  Absorption of Azulene: Femtosecond Transient Spectra and Excited State Calculations.
131. P. Cronstrand, O. Christiansen, P. Norman, and H. Ågren, *Phys. Chem. Chem. Phys.*, **2**, 5357 (2000). Theoretical Calculations of Excited State Absorption.
132. Y. H. Meyer, R. Astier, and J. M. Leclercq, *J. Chem. Phys.*, **56**, 801 (1972). Triplet-Triplet Spectroscopy of Polyacenes.
133. G. Snatzke, *Angew. Chem.*, **91**, 380 (1979). Circular dichroismus und Absolute Konfiguration: Anwendung der Qualitativen MO-Theorie auf die Chiroptischen Phänomene.
134. L. A. Neubert and M. Carmack, *J. Am. Chem. Soc.*, **96**, 943 (1974). Circular Dichroism of Disulfides with Dihedral Angles of 0, 30 and 60 deg. in the 400–185 nm Spectral Region.
135. V. O. Saik and S. Lipsky, *J. Phys. Chem. A*, **105**, 10107 (2001). Absorption Spectra of Some Liquids in the VUV.
136. F. Furche, R. Ahlrichs, C. Wachsmann, E. Weber, A. Sobanski, F. Vögtle, and S. Grimme, *J. Am. Chem. Soc.*, **122**, 1717 (2000). Circular Dichroism of Helicenes Investigated by Time-Dependent Density Functional Theory.

137. W. S. Brickell, A. Brown, C. M. Kemp, and S. F. Mason, *J. Chem. Soc (A)*., 756 (1971).  $\pi$  Electron Absorption and Circular Dichroism Spectra of [6]- and [7]-Helicene.
138. D. Gruner, A. Nguyen, and P. Brumer, *J. Chem. Phys.*, **101**, 10366 (1994). Theoretical Study of the  $S_1$ - $S_0$  Spectroscopy of Anthracene.
139. P. R. Callis, J. T. Vivian, and L. S. Slater, *Chem. Phys. Lett.*, **244**, 53 (1995). Ab Initio Calculations of Vibronic Spectra for Indole.
140. F. Furche and R. Ahlrichs, *J. Chem. Phys.*, **117**, 7433 (2002). Adiabatic Time-Dependent Density Functional Methods for Excited State Properties.
141. M. Odellius, D. Laikov, and J. Hutter, *J. Mol. Struct.*, **630**, 163 (2003). Excited State Geometries within Time-Dependent and Restricted Open-Shell Density Functional Theories.
142. S. Hirata and M. Head-Gordon, *Chem. Phys. Lett.*, **302**, 375 (1999). Time-Dependent Density Functional Theory for Radicals. An Improved Description of Excited States with Substantial Double Excitation Character.
143. M. E. Casida, K. C. Casida, and D. R. Salahub, *Int. J. Quant. Chem.*, **70**, 933 (1998). Excited-State Potential Energy Curves From Time-Dependent Density-Functional Theory: A Cross Section of Formaldehydes  $^1A_1$  Manifold.
144. J. D. Rogers, *J. Phys. Chem.*, **94**, 4011 (1990). Ultraviolet Absorption Cross Sections and Atmospheric Photodissociation Rate Constant of Formaldehyde.
145. D. C. Moule and A. D. Walsh, *Chem. Rev.*, **75**, 67 (1975). Ultraviolet Spectra and Excited States of Formaldehyde.
146. R. Ahlrichs, M. Bär, H.-P. Baron, R. Bauernschmitt, S. Böcker, M. Ehrig, K. Eichkorn, S. Elliott, F. Furche, F. Haase, M. Häser, H. Horn, C. Huber, U. Huniar, M. Kattannek, C. Kölmel, M. Kollwitz, K. May, C. Ochsenfeld, H. Öhm, A. Schäfer, U. Schneider, O. Treutler, M. von Arnim, F. Weigend, P. Weis, and H. Weiss. TURBOMOLE (Ver. 5.6), Universität Karlsruhe, 2003.